Please cite this article in press as: Choe et al., Glycolysis model shows that allostery maintains high ATP and limits accumulation of intermediates, Biophysical Journal (2025), https://doi.org/10.1016/j.bpj.2025.03.037

Biophysical Journal
Article

Biophysical Society

Glycolysis model shows that allostery maintains high ATP and limits accumulation of intermediates

Mangyu Choe,[1,2] Tal Einav,[4,6,7] Rob Phillips,[4,5] and Denis V. Titov[1,2,3,*]

[1]Department of Nutritional Sciences and Toxicology, University of California, Berkeley, Berkeley, California; [2]Department of Molecular and Cell Biology, University of California, Berkeley, Berkeley, California; [3]Center for Computational Biology, University of California, Berkeley, Berkeley, California; [4]Division of Biology and Biological Engineering, California Institute of Technology, Pasadena, California; [5]Department of Physics, California Institute of Technology, Pasadena, California; [6]Basic Sciences Division and Computational Biology Program, Fred Hutchinson Cancer Research Center, Seattle, Washington; and [7]Center for Vaccine Innovation, La Jolla Institute for Immunology, La Jolla, California

ABSTRACT Glycolysis is a conserved metabolic pathway that produces ATP and biosynthetic precursors. It is not well understood how the control of mammalian glycolytic enzymes through allosteric feedback and mass action accomplishes various tasks of ATP homeostasis, such as controlling the rate of ATP production, maintaining high and stable ATP levels, ensuring that ATP hydrolysis generates a net excess of energy, and maintaining glycolytic intermediate concentrations within physiological levels. To investigate these questions, we developed a biophysical model of glycolysis based on enzyme rate equations derived from in vitro kinetic data. This is the first biophysical model of human glycolysis that successfully recapitulates the above tasks of ATP homeostasis and predicts absolute concentrations of glycolytic intermediates and isotope tracing kinetics that align with experimental measurements in human cells. We use the model to show that mass action alone is sufficient to control the ATP production rate and maintain the high energy of ATP hydrolysis. Meanwhile, allosteric regulation of hexokinase and phosphofructokinase by ATP, ADP, inorganic phosphate, and glucose-6-phosphate is required to maintain high ATP levels and to prevent uncontrolled accumulation of phosphorylated intermediates of glycolysis. Allosteric feedback achieves the latter by maintaining hexokinase and phosphofructokinase enzyme activity at one-half of ATP demand and, thus, inhibiting the reaction of Harden and Young, which otherwise converts glucose to supraphysiological levels of phosphorylated glycolytic intermediates at the expense of ATP. Our methodology provides a roadmap for a quantitative understanding of how metabolic homeostasis emerges from the activities of individual enzymes.

SIGNIFICANCE Metabolic homeostasis maintains appropriate levels of energy and biosynthetic precursors under variable conditions. To achieve this, metabolic pathways are regulated by a combination of mass action and allosteric feedback. We have extensive knowledge of the molecular details of the allosteric regulation of many individual enzymes, but our understanding of how metabolic homeostasis emerges from the activities of individual enzymes is incomplete, and the number of allosteric regulators that remain to be discovered is unknown. Here, we use a combination of theory and experiments to identify the function of several conserved allosteric regulators of the glycolysis pathway. Our methodology can be applied to any other metabolic pathway and provide a framework for quantitative understanding of cellular metabolic homeostasis.

INTRODUCTION

Glycolysis is conserved across all domains of life. This key pathway harnesses the breakdown of glucose to produce energy in the form of ATP and precursors for the biosynthesis of amino acids, nucleotides, carbohydrates, and lipids. Glycolysis produces ATP both directly by a process referred to as fermentation or aerobic glycolysis (Fig. 1 *A*) and indirectly by producing pyruvate, which is used as a substrate for ATP generation by respiration. The net reaction of mammalian aerobic glycolysis converts extracellular glucose to extracellular lactic acid, while the only net intracellular reaction is the production of ATP from ADP and inorganic phosphate (Fig. 1 *A*). Aerobic glycolysis is the most active metabolic pathway in proliferating mammalian cells (an observation known as the Warburg effect (1)), able to satisfy all the ATP demand even in the absence of

Submitted December 24, 2024, and accepted for publication March 31, 2025.

*Correspondence: titov@berkeley.edu

Editor: Margaret Johnson.

https://doi.org/10.1016/j.bpj.2025.03.037

Please cite this article in press as: Choe et al., Glycolysis model shows that allostery maintains high ATP and limits accumulation of intermediates, Biophysical Journal (2025), https://doi.org/10.1016/j.bpj.2025.03.037

respiration (2,3). The reliance of proliferating mammalian cells on aerobic glycolysis for ATP production and the lack of intracellular products except for ATP makes glycolysis a convenient self-contained system for studying ATP homeostasis.

To maintain ATP homeostasis, the glycolysis pathway must simultaneously achieve several tasks, such as regulating the rate of ATP production, ensuring that the ATP hydrolysis reaction generates a net excess of energy, maintaining most of the adenine nucleotide pool in the form of ATP, balancing the activity of glycolysis with other metabolic pathways, and maintaining intermediate concentrations within a physiological range. These tasks must be achieved at a wide range of ATP demands and be robust to small variations in enzyme concentrations and kinetic parameters that are observed due to the stochasticity of gene expression or physiological changes in temperature or pH. The impressive capabilities of the glycolysis control system are evident in its ability to maintain ATP and glycolytic intermediate concentrations within a narrow 2- to 3-fold range in response to a more than 100-fold change in ATP demand (4–6).

Glycolytic ATP homeostasis is an emergent property of the activities of individual enzymes that are controlled by a combination of mass action and allosteric regulation. Mass action involves the regulation of enzyme rate in response to changes in substrate and product concentrations. Allosteric regulation (7–11) refers to the modulation of enzyme kinetic properties by metabolite binding or posttranslational modifications, allowing for feedback regulation to achieve the desired properties of homeostasis by modifying the mass action trends of biochemical reactions (12–14). Decades of biochemical studies with purified enzymes have uncovered that four glycolytic enzymes—hexokinase (HK), phosphofructokinase (PFK), glyceraldehyde-3-dehydrogenase (GAPDH), pyruvate kinase (PK)—are allosterically regulated by a constellation of metabolites such as ATP, ADP, AMP, inorganic phosphate, and other regulators (Fig. 1, *A* and *B*). To date, the consequences of disrupting these allosteric interactions on the glycolytic pathway activity have not been experimentally investigated. This is likely due to the practical difficulty of simultaneously deleting or mutating a minimum of 10 genes encoding various human isoforms of HK, PFK, GAPDH, and PK. Therefore, the roles of mass action and allostery in the control of specific tasks of glycolytic ATP homeostasis are unknown.

Due to the complexity of ATP homeostasis and the challenges in experimentally disabling allosteric feedback, much of the understanding of how allostery and mass action regulate glycolytic activity has come from mathematical models. These studies typically employed simplified models of glycolysis involving two to three enzymes to enable the use of analytical techniques. They provided three key insights into the role of mass action and allostery in controlling glycolysis. First, mass action alone can, in principle, regulate several aspects of glycolysis without the need for allosteric regulators, such as controlling the ATP production rate, maintaining high ATP levels in response to varying demands, and even enabling oscillations of intermediates (15). One study suggested that glycolysis, in isolation, might not require allosteric regulation to maintain ATP homeostasis, and that allostery may have evolved primarily to coordinate glycolysis with other metabolic pathways (16). Second, the structure of glycolysis—where ATP is consumed initially and later produced in greater amounts—could result in overactive ATP hydrolysis by HK and PFK reactions and the accumulation of phosphorylated intermediates (17), as observed in cell-free systems (18,19) and perturbed living cells (20–22). Investigation of the three-enzyme model of glycolysis revealed that feedback inhibition of HK by G6P can prevent this issue (17), but reducing HK levels could also achieve a similar effect, suggesting that feedback inhibition of HK by G6P may only be necessary under high glucose conditions (17). Third, allosteric activation of PFK by F16BP or AMP might be required for generating oscillations of glycolytic intermediates (23–25), which have been observed experimentally after perturbations (26,27). However, it remains unclear whether these oscillations are physiologically relevant or simply a byproduct of allosteric feedback serving other roles (25). Despite the progress made in exploring the potential roles of allosteric regulators of glycolytic enzymes, their precise function remains unclear. Importantly, while coarse-grained models allow the use of powerful analytical techniques, they may omit the very components that necessitate allosteric feedback. More detailed models of glycolysis, which include all relevant enzymes and utilize experimentally derived kinetic and thermodynamic parameters, have been developed (28–31), but their behavior with and without allosteric regulation has not been investigated.

Here, we investigated the role of mass action and allostery in controlling various tasks of glycolytic ATP homeostasis using a combination of theory and experiments. The core of our approach is a mathematical model that uses enzyme rate equations to simulate the activity of all glycolytic enzymes using a system of ordinary differential equations (ODEs). The model uses enzyme isoforms, enzyme concentrations, and cofactor pool concentrations observed in proliferating normal and cancer human cell lines. The key components of our model are the newly derived rate equations for allosterically regulated enzymes HK, PFK, GAPDH, and PK based on decades of in vitro kinetic data. To the best of our knowledge, we compiled the largest dataset of mammalian glycolytic enzyme kinetic data reported to date, comprising about 3000 measurements (Data S2). We used the Monod-Wyman-Changeux (MWC) model (9–11,32,33) in combination with rigorous statistical approaches to identify the relevant rate equations and estimate the kinetic constants using a manually curated dataset of thousands of data points from dozens of publications. We

Please cite this article in press as: Choe et al., Glycolysis model shows that allostery maintains high ATP and limits accumulation of intermediates, Biophysical Journal (2025), https://doi.org/10.1016/j.bpj.2025.03.037

solved a difficult problem of parameter estimation of a large mechanistic model by fully constraining our model with 172 parameters estimated independently based on proteomics, metabolomics, and in vitro kinetics data from dozens of datasets. Our model robustly performed the key tasks of glycolytic ATP homeostasis and predicted absolute concentrations of glycolytic intermediates, reaction disequilibrium ratios, and isotope tracing consistent with measurements in living cells. Analysis of our model showed that allosteric regulation of HK and PFK is required to maintain high ATP levels and to prevent uncontrolled accumulation of phosphorylated intermediates of upper glycolysis. Allosteric feedback achieves the latter by maintaining HK and PFK enzyme activity at one-half of ATP demand and, thus, inhibiting the reaction of Harden and Young (18,19), which otherwise converts glucose to supraphysiological levels of phosphorylated glycolytic intermediates at the expense of ATP. Mass action performed other tasks of glycolytic ATP homeostasis previously attributed to allostery, such as controlling the rate of ATP production to match ATP supply and demand, and maintaining ATP, ADP, and inorganic phosphate levels such that ATP hydrolysis reaction generates energy.

MATERIALS AND METHODS

Estimation of intracellular concentrations of glycolytic enzymes

We estimated the abundance of glycolytic enzymes in mammalian cell lines using publicly available proteomics data (34). We first used proteomics data to calculate the fraction a specific glycolytic enzyme occupies compared with total proteome size as a ratio of peptide intensities for the specific glycolytic enzyme to total peptide intensity for all proteins. This approach has been shown to produce good estimates of absolute protein amounts (35). Values of mg protein per mg total protein were then converted to concentration using the molecular weight of each enzyme and the cellular protein density of ∼200 mg/mL (36). The resulting dataset of glycolytic enzyme concentrations is reported in Data S1. In the model simulations, we further converted whole-cell enzyme concentrations from Data S1 to cytosolic enzyme concentrations as glycolytic enzymes are localized to the cytosol. We estimated that the enzymes of glycolysis are concentrated in a volume that is ∼50% of cellular volume, as ∼70% of the cell is cytosol (37) and ∼70% of the cytosol is water (38,39).

Measurement of intracellular glycolytic intermediate concentrations using LC-MS

LC-MS was used to profile and quantify the polar metabolite contents of whole-cell samples. The metabolite extraction buffer was composed of 40% methanol (Fisher Scientific [Waltham, MA], cat. no. A456-4) and 40% acetonitrile (Fisher Scientific, cat. no. A9554) in water (Fisher Scientific, cat. no. W64) containing 0.1 M formic acid (Fisher Scientific, cat. no. A11750), supplemented with a mixture of 8 isotope-labeled chemicals at 1 μM (ATP [Sigma, Burlington, MA, cat. no. 710695], AMP [Sigma, cat. no. 900382], glucose-6-phosphate [Cambridge Isotope Laboratories [Cambridge, MA], cat. no. CLM-8367), and fructose-6-phosphate (F6P) (Cambridge Isotope Laboratories, cat. no. CLM-8616]), 10 μM (lactate [Sigma, cat. no. 490040], pyruvate [Sigma, cat. no. 490709], and fructose-1,6-bisphosphate [Cambridge Isotope Laboratories, cat. no. CLM-3398]) or 20 μM (glucose [Sigma, cat. no. 389374]), which were used as internal standards.

Metabolite analysis was performed on an Agilent (Santa Clara, CA) 6430 Triple Quad interfaced with an Agilent 1260 Infinity II LC system. Five microliters of each metabolite sample was injected onto a SeQuant ZIC-pHILIC column 5 μm polymer 150 × 2.1 mm (Millipore/Sigma, cat. no. 1504600001). Buffer A was 100% acetonitrile; buffer B was 20 mM ammonium carbonate, 0.1% ammonium hydroxide. The chromatographic gradient was run at a flow rate of 0.150 mL/min as follows: 0–0.5 min: hold at 80% A; 0.5–30.5 min: linear gradient from 80 to 20% A; 30.5–30.8 min: hold at 20% A; 30.8–31 min: linear gradient from 20 to 80% A; 31–60 min: hold at 80% A.

The MS settings were kept consistent regardless of the chromatographic separation being tested. MS parameters were as follows: gas, 350°C at 11 L/min; nebulizer, 35 psi at 4000 V. The MS was operated in negative ionization mode for all samples analyzed.

All experiments were performed in replicates of five ($n = 5$) per sample group. Metabolite identification and quantification were performed with the Agilent MassHunter Qualitative Analysis software (version B.06.00). To confirm metabolite identities and to enable quantification, the pools of metabolite standards were used. To accurately quantify target metabolites, the final concentrations of standards were 100, 50, 25, 12.5, 6.25, 3.125, and 1.56 μM, 781, 390, 195, 97, and 49 nM. In each sample, the raw peak area of each metabolite was divided by the raw peak area of the relevant isotope-labeled internal standard to calculate the absolute concentration. ATP, AMP, glucose-6-phosphate, fructose-1,6-bisphosphate, pyruvate, and lactate were normalized with their isotope-labeled counterparts. For determining the absolute concentrations of all other metabolites, the peak areas were normalized with two isotope-labeled internal standards that have the closest retention time. The raw peak area values were fit to a linear fitting curve equation, typically with $r^2 > 0.99$, which was then used to calculate the concentration of the metabolite in each extract. The final intracellular concentrations of target metabolites were then calculated from the sample dilution-fold and the corresponding cell volume, which was estimated using the Beckman Z2 Coulter Counter.

Two sets of isomers, F6P/glucose-1-phosphate (G1P) and 3-phosphoglycerate/2-phosphoglycerate were not separated under our chromatographic conditions. We took advantage of the different ratios of the signal from two transition states for each of the isomers to deconvolve the peaks. For example, F6P and G1P generate different signal ratios from two transition states with product ion values of 78.96 or 96.97. We used F6P and G1P standards to determine the ratios of signal from 78.96 product ion to that of 96.97 product ion and used these values to deconvolve the peaks containing the mixture of the two compounds.

One million C2C12 or HeLa cells were seeded on 6-well plates in 2 mL of DMEM without pyruvate (US Biological [Salem, MA], cat. no. D9802-25L), supplemented with 25 mM glucose, 3.7 g/L $NaHCO_3$, and 10% FBS (Gibco, cat. no. 10437028). Twenty-four hours later, the medium was exchanged to 2 mL of DMEM medium without pyruvate, supplemented with 25 mM glucose, 3.7 g/L $NaHCO_3$, 10% FBS, and 1 μM oligomycin (MP Biomedicals [Santa Ana, CA], cat. no. 151786). Metabolite extraction was performed on ice. After 2 h incubation, the cell culture plate was placed on ice and the medium was aspirated. One hundred and fifty microliters of ice-chilled extraction buffer (40:40:20, methanol/acetonitrile/water) containing 0.1 M formic acid and 8 isotope-labeled internal standards was added and cells were scraped with a cell lifter for 10 s. The lysate was transferred to a 1.5-mL tube on ice. Five minutes later, cells were centrifuged at 17,000 × g at 4°C for 10 min. Supernatants were collected and neutralized by adding ammonium bicarbonate (final concentration of 100 mM). These samples were analyzed with LC-MS as described above to determine intracellular concentrations of metabolites.

For each experiment, a replicate set of cells was treated identically in parallel and used for measuring cell number and volume. The contents of each well were trypsinized, and cell number and volume were measured using a

Please cite this article in press as: Choe et al., Glycolysis model shows that allostery maintains high ATP and limits accumulation of intermediates, Biophysical Journal (2025), https://doi.org/10.1016/j.bpj.2025.03.037

Beckman Z2 Coulter Counter with a size setting of 492.8–23620 fL. Intracellular concentrations were calculated using the total number of cells per sample and the volume of each cell.

Estimates of glycolytic intermediate concentrations from the literature

In addition to our own measurements of glycolytic intermediate concentrations, we have compiled a dataset of mammalian glycolytic concentrations measured under different conditions from eight publications (29,31,40–45). The resulting dataset combined with our own measurement is reported in Fig. 2 *E* and provided in Data S1. In Fig. 2 *E*, we further converted whole-cell metabolite concentrations from Data S1 to cytosolic metabolite concentrations as glycolysis is localized to the cytosol. We estimated that the metabolites of glycolysis are concentrated in a volume that is ∼50% of cellular volume, as ∼70% of the cell is cytosol (37) and ∼70% of the cytosol is water (38,39).

Measurement of glycolytic fluxes using [^{13}C] glucose and [^{13}C]lactate

C2C12 or HeLa cells (1 million) were seeded on 6-well plates in 2 mL of DMEM without pyruvate, supplemented with 25 mM glucose, 3.7 g/L $NaHCO_3$, and 10% FBS. Twenty-four hours later, the medium was exchanged to 2 mL of DMEM medium without pyruvate, supplemented with 25 mM glucose, 3.7 g/L $NaHCO_3$, 10% FBS, and 1 μM oligomycin. After 2 h incubation, the medium was exchanged to 2 mL of DMEM medium without pyruvate, supplemented with 25 mM [$^{13}C_6$]glucose (Sigma [Burlington, MA], cat. no. 389274-1G), 3.7 g/L $NaHCO_3$, 10% dialyzed FBS (ThermoFisher [Waltham, MA], cat. no. 26400044), and 1 μM oligomycin or 2 mL of DMEM medium without pyruvate, supplemented with 25 mM glucose, 5 mM [$^{13}C_3$]lactate (Cambridge Isotope Laboratories [Cambridge, MA], cat. no. CLM-1579-N-0.1MG), 3.7 g/L $NaHCO_3$, 10% dialyzed FBS, and 1 μM oligomycin. After 1, 3, 10, and 30 min, cell culture plates were placed on ice and medium was aspirated. Cells were rinsed with 2 mL of ice-cold 100 mM ammonium bicarbonate for no more than 10 s and metabolites were extracted as described above using extraction buffer (40:40:20, methanol/acetonitrile/water) containing 0.1 M formic acid and 1 μM isotopic AMP. In each sample, the raw peak area of each metabolite was divided by the raw peak area of isotope-labeled AMP internal standard to calculate the relative abundance.

Numerical simulations of differential equations constituting the glycolysis model

The glycolysis model is a system of ODEs. The number of equations is equal to the number of metabolites, and each equation consists of a derivative of metabolite concentration with respect to time being equal to the sum of enzyme rates producing the metabolite minus the sum of enzyme rates consuming the metabolite:

$$\begin{aligned}
\frac{d[Glucose_{media}]}{dt} &= 0 \\
\frac{d[Glucose]}{dt} &= V^{GLUT} - V^{HK1} \\
\frac{d[G6P]}{dt} &= V^{HK1} - V^{GPI} \\
\frac{d[F6P]}{dt} &= V^{GPI} - V^{PFKP} \\
\frac{d[F16P]}{dt} &= V^{PFKP} - V^{ALDO} \\
\frac{d[GAP]}{dt} &= V^{ALDO} + V^{TPI} - V^{GAPDH} \\
\frac{d[DHAP]}{dt} &= V^{ALDO} - V^{TPI} \\
\frac{d[BPG]}{dt} &= V^{GAPDH} - V^{PGK} \\
\frac{d[3PG]}{dt} &= V^{PGK} - V^{PGAM} \\
\frac{d[2PG]}{dt} &= V^{PGAM} - V^{ENO} \\
\frac{d[PEP]}{dt} &= V^{ENO} - V^{PKM2} \\
\frac{d[Pyruvate]}{dt} &= V^{PKM2} - V^{LDH} \\
\frac{d[Lactate]}{dt} &= V^{LDH} - V^{MCT} \\
\frac{d[Lactate_{media}]}{dt} &= 0 \\
\frac{d[ATP]}{dt} &= -V^{HK1} - V^{PFKP} + V^{PGK} + V^{PKM2} + V^{AK} \\
&\quad - V^{ATPase} \\
\frac{d[ADP]}{dt} &= V^{HK1} + V^{PFKP} - V^{PGK} - V^{PKM2} - 2V^{AK} \\
&\quad + V^{ATPase} \\
\frac{d[AMP]}{dt} &= V^{AK} \\
\frac{d[Phosphate]}{dt} &= V^{ATPase} - V^{GAPDH} \\
\frac{d[NADH]}{dt} &= V^{GAPDH} - V^{LDH}
\end{aligned} \tag{1}$$

Please cite this article in press as: Choe et al., Glycolysis model shows that allostery maintains high ATP and limits accumulation of intermediates, Biophysical Journal (2025), https://doi.org/10.1016/j.bpj.2025.03.037

$$\frac{d[NAD]}{dt} = V^{LDH} - V^{GAPDH}$$

The ODE model can also be represented in the form of the stoichiometric matrix.

observed in live cells. DifferentialEquations.jl has callback capabilities, which allowed us to change any parameter of the model (e.g., ATPase rate or concentration of any metabolite) at any time during the simulation. A typical simulation took 2–20 ms on a single core of Apple M1 Max processor, which allowed us to test many different conditions in a short period of time using a personal computer.

	GLUT	HK1	GPI	PFKP	ALDO	TPI	GAPDH	PGK	PGM	ENO	PKM2	LDH	MCT	ATPase	AK
Media Glucose	0	0	0	0	0	0	0	0	0	0	0	0	0	0	0
Glucose	1	−1	0	0	0	0	0	0	0	0	0	0	0	0	0
G6P	0	1	−1	0	0	0	0	0	0	0	0	0	0	0	0
F6P	0	0	1	−1	0	0	0	0	0	0	0	0	0	0	0
F16BP	0	0	0	1	−1	0	0	0	0	0	0	0	0	0	0
GAP	0	0	0	0	1	1	−1	0	0	0	0	0	0	0	0
DHAP	0	0	0	0	1	−1	0	0	0	0	0	0	0	0	0
BPG	0	0	0	0	0	0	1	−1	0	0	0	0	0	0	0
3PG	0	0	0	0	0	0	0	1	−1	0	0	0	0	0	0
2PG	0	0	0	0	0	0	0	0	1	−1	0	0	0	0	0
PEP	0	0	0	0	0	0	0	0	0	1	−1	0	0	0	0
Pyruvate	0	0	0	0	0	0	0	0	0	0	1	−1	0	0	0
Lactate	0	0	0	0	0	0	0	0	0	0	0	1	−1	0	0
Media Lactate	0	0	0	0	0	0	0	0	0	0	0	0	0	0	0
ATP	0	−1	0	−1	0	0	0	1	0	0	1	0	0	−1	1
ADP	0	1	0	1	0	0	0	−1	0	0	−1	0	0	1	−2
AMP	0	0	0	0	0	0	0	0	0	0	0	0	0	0	1
Phosphate	0	0	0	0	0	0	−1	0	0	0	0	0	0	1	0
NAD	0	0	0	0	0	0	−1	0	0	0	0	1	0	0	0
NADH	0	0	0	0	0	0	1	0	0	0	0	−1	0	0	0

The stoichiometric matrix allows us to calculate the number of conserved moieties and identify them using chemical reactions network theory. The number of conserved moieties is the number of metabolites (i.e., rows) minus the rank of the stoichiometric matrix, and the conserved moieties are the left null space of the stoichiometric matrix. The six conserved moieties are.

1) adenine pool: ATP + ADP + AMP
2) NAD(H) pool: NAD + NADH
3) media glucose
4) media lactate
5) total phosphate pool: PEP + 2PG + DHAP + phosphate + GAP + 2.0F16BP + ADP + 3PG + F6P + G6P + 2.0BPG + 2.0ATP
6) redox state of intermediates: NADH – pyruvate – PEP – 2PG – 3PG – BPG

We numerically simulated Eq. 13 using the DifferentialEquations.jl library (46) and plotted the result using Makie.jl library (47). We used Rodas5P solver for stiff differential equations with 10^{-15} absolute tolerance and 10^{-8} relative tolerance for most simulations and RadauIIA5 solver for simulations with constant phosphate and simulations where rate equations for HK1 and PFKP were substituted for one-half of ATPase rate equations. Tolerances were chosen to provide minimal numerical errors estimated by Uncertainty Quantification callback AdaptiveProbIntsUncertainty from the DiffEqCallbacks.jl library. Numerical simulation of ODEs requires an initial condition consisting of metabolite concentration at time 0. We used estimates of intracellular concentrations of glycolytic intermediates as initial conditions (see Data S1) or a steady-state solution for dynamic simulations with step responses to changes in ATPase rate. A large range of initial conditions, including all metabolites being zero except for ATP, NAD, and extracellular glucose, produced similar steady-state solutions as shown in Fig. S1, *G–I*. We simulated differential equations for 10^8 s (∼3.2 years) to find the steady-state concentrations of metabolites. Typically, the solution was close to steady state after only several seconds in accordance with a rapid rate of glycolysis

Calculation of ATP turnover, energy released by ATP hydrolysis, bound and free metabolite concentrations

The output of the simulation of Eq. 1 is the free concentrations of metabolites at every time point starting from initial conditions. This output can be used to calculate many properties of the glycolysis pathway, such as rates of any reaction or concentrations of bound metabolites, by plugging metabolite concentration into enzyme rate equations described in the supporting material.

Consumption and production of ATP was calculated using the following equations:

$$ATP\ consumption = V^{ATPase} \quad (2)$$

$$ATP\ production = V^{PGK} + V^{PKM2} + V^{AK} - V^{HK1} - V^{PFKP} \quad (3)$$

Energy released by ATP hydrolysis in units of k_BT was calculated using the following equation:

$$E^{ATPase} = -ln\left(\frac{\Gamma}{K_{eq}}\right) = -ln\left(\frac{\frac{[ADP][Phosphate]}{[ATP]}}{K_{eq}}\right) \quad (4)$$

where Γ is the mass action ratio of ATP hydrolysis and K_{eq} is the equilibrium constant of ATP hydrolysis.

The concentration of enzyme-bound metabolites was calculated using binding equations described in the supporting material. Accounting for enzyme-bound metabolites is essential to ensure an accurate comparison of model prediction to whole-cell measurements as the latter represents a sum of enzyme-bound and free metabolites. Intracellular concentrations of glycolytic

Please cite this article in press as: Choe et al., Glycolysis model shows that allostery maintains high ATP and limits accumulation of intermediates, Biophysical Journal (2025), https://doi.org/10.1016/j.bpj.2025.03.037

enzymes are 1–10 μM, which is comparable with intracellular concentrations of some glycolytic intermediates. Therefore, some of the metabolites are mostly present in an enzyme-bound state, and their concentrations will be underestimated by the model without accounting for the enzyme-bound fraction.

Estimation of uncertainty of model predictions

Outputs of the glycolysis model have uncertainty due to uncertainty of estimates of model parameters such as kinetic constants, thermodynamic constants, and enzyme concentrations. Understanding the uncertainty of model predictions is important for quantitative comparisons of model predictions to data and for understanding the robustness of model predictions. We used bootstrapping to calculate the uncertainty of glycolysis model predictions. We rerun the model 10,000 times using different sets of parameter values, where each parameter value is generated by randomly drawing a value from a normal distribution with a mean and standard deviation corresponding to the mean and standard deviation of that parameter estimate. We bootstrapped all the parameters except we kept the kinetic parameters of ATPase and adenylate kinase unchanged during bootstrapping as these enzymes are not part of glycolysis and we set V_{max} of ATPase to be equal to a fraction of V_{max} of HK1 or V_{max} PFKP, whichever was smaller in a particular bootstrapped parameter set. In most analyses, we only reported the data from bootstrapped simulations that could match ATP supply and demand as indicated in relevant figure legends because including simulations that come to equilibrium due to the inability to produce ATP fast enough is not informative as they represent a completely different state of the glycolysis system akin to a dead cell. In summary, this general bootstrapping approach allows us to estimate the uncertainty of any output of our model.

Global sensitivity analysis

Sensitivity analysis is a set of powerful approaches aimed to systematically explore the role of specific parameters of an ODE model in controlling specific outputs of the model, such as maintenance of high ATP level at a range of ATP turnovers, prediction of metabolite concentration, speed of the response to perturbation, etc. Sensitivity analysis can be broadly subdivided into local sensitivity analysis and global sensitivity analysis methods. Local sensitivity analysis methods using partial derivates were historically more popular, especially for simple models where analytical derivatives can be calculated. When applied to models of metabolic pathways, local sensitivity analysis is sometimes referred to as metabolic control analysis (48,49). The limitations of local sensitivity analysis are that it only considers the effect of one parameter at a time (i.e., ignores interactions between parameters) and only estimates the role of the parameter at a specific value of that parameter and every other parameter (i.e., local). To overcome these limitations, global sensitivity analysis methods were developed that allow systematic evaluation of parameter importance at a large range of parameter values (i.e., global) and that can estimate the effect of interactions between parameters. The only limitation of variance decomposition methods is that they are much more computationally intensive than local sensitivity analysis methods, which limited their use before the early 2000s when the computational power caught up to the demands of these methods.

We used a global sensitivity analysis method called variance decomposition to learn about the role of specific model parameters in controlling specific outputs of our model. Here, we briefly describe the idea behind this method and refer the reader to several excellent books that have been written about global sensitivity analysis for more in-depth discussion (50,51). First, we chose a scalar output Y of the model that we want to investigate. We focused on investigating the model parameters required to maintain high ATP concentration, high energy of ATP hydrolysis, and the ability of model to match ATP production and ATP consumption rates. Then we perform repeated simulations of the model using different starting parameters drawn from a log-uniform distribution with values threefold lower to threefold higher than the model values. We then calculated how much each parameter or combination of parameters contributes to the variance of output Y observed during repeated simulations. A parameter that is important for controlling Y will have a large contribution, and the parameter that is not important will have small or no contributions. The variance of output Y that depends on k input parameters P could be uniquely decomposed into the following terms:

$$Var(Y) = \sum_i V_i + \sum_i \sum_{j>i} V_{ij} + \sum_i \sum_{j>i} \sum_{l>j} V_{ijl} + \ldots + V_{1,2\ldots k} \tag{5}$$

where

$$V_i = Var(E(Y|P_i))$$

$$V_{i,j} = Var\big(E\big(Y\big|P_i,P_j\big)\big) - V_i - V_j$$

$$V_{i,j,l} = Var\big(E\big(Y\big|P_i,P_j,P_l\big)\big) - V_i - V_j - V_l - V_{i,j} - V_{i,l} - V_{j,l}$$

Two types of sensitivity indexes, S_i and S_i^T, are useful in analyzing the contribution of input parameters. S_i is called sensitivity index, importance measure or first-order effect:

$$S_i = \frac{V_i}{Var(Y)} \tag{6}$$

Another way to understand S_i is that it is a fraction of the variance of Y that would disappear if we fixed parameter P_i at some value. Parameter P_i would be considered important for controlling output Y if fixing its value would lead to a large reduction of the variance of Y (i.e., S_i is large). S_i has several nice properties where for an additive model $\sum S_i = 1$ and for any model with independent input parameters $\sum S_i \leq 1$. For example, a large value of $1 - \sum S_i$ indicates that interactions between parameters are important for controlling a specific output of the model. More generally, for any model with independent input parameters:

$$\sum_i S_i + \sum_i \sum_{j>i} S_{ij} + \sum_i \sum_{j>i} \sum_{l>j} S_{ijl} + \ldots + S_{1,2\ldots k} = 1 \tag{7}$$

S_i^T is called the total-order effect and contains all terms in Eq. 7 that contain i:

$$S_i^T = 1 - \frac{Var(E(Y|P_{-i}))}{Var(Y)} = \frac{E(Var(Y|P_{-i}))}{Var(Y)} = S_i + \sum_{j\neq i} S_{ij} + \sum_{l\neq i,j} \sum_{j\neq i} S_{ijl} + \ldots \tag{8}$$

Another way to understand S_i^T is that it is a fraction of the variance of Y that would be left if we fixed all parameters except parameter P_i at some value. Parameter P_i would be considered important for controlling output Y if fixing all the parameters except P_i at some value would still leave a large fraction of variance of Y (i.e., S_i^T is large). Unlike S_i, $\sum S_i^T$ can be larger or smaller than 1 and Eq. 7 does not hold for S_i^T because S_i^T and S_j^T would have one or several overlapping terms (e.g., S_{ij}).

We have calculated S_i and S_i^T for various outputs of the model using the Sobol method of the GlobalSensitivity.jl package (52).

Please cite this article in press as: Choe et al., Glycolysis model shows that allostery maintains high ATP and limits accumulation of intermediates, Biophysical Journal (2025), https://doi.org/10.1016/j.bpj.2025.03.037

Adoption of the glycolysis model for simulation of [U-^{13}C]glucose and [U-^{13}C]lactate tracing

Glycolysis model can be used to predict the results of heavy isotope tracing experiments. To predict tracing patterns, we decompose each rate equation into enzyme activity part and mass action part as described previously (12,53,54):

$$V = Enzyme\ Activity \cdot \left([S_1] \cdot [S_2] - \frac{[P_1] \cdot [P_2]}{Keq} \right) \quad (9)$$

Enzyme activity depends on the total concentration of metabolites (i.e., sum of all isotopomers), while the mass action part is responsible for the propagation of the isotope label. Therefore, for modeling isotope tracing, we modify all kinetic equations to be able to use heavy and light isotope-labeled metabolites that we incorporate in the mass action part of all the equations, and we double the number of ODEs to account for time-dependent changes of both heavy and light isomers (i.e., we have one ODE for each isotope).

Kinetic equations and numerical simulation of differential equations constituting the two-enzyme model

We described the kinetics of enzyme 1, enzyme 2, and ATPase using simplified rate equations. We started from reversible Michaelis-Menten equations (54) for enzyme 2 and ATPase. For enzyme 1, we used the MWC model to add allosteric activation by ADP and phosphate and allosteric inhibition by ATP. We assumed that ADP and phosphate only bind to active conformation, ATP only binds to inactive conformation, inactive MWC conformation of enzyme 1 is catalytically inactive. The resulting complete rate equations for enzyme 1, enzyme 2, and ATPase are:

$$V^{Enz\ 1} = \frac{V_{max}^{Enz\ 1}}{1 + \frac{L\left(1 + \frac{[ATP]}{K_I^{ATP}}\right)^n}{\left(1 + \frac{[ADP]}{K_A^{ADP}}\right)^n \left(1 + \frac{[Phosphate]}{K_A^{Phosphate}}\right)^n}} \left(\frac{\frac{[G][ATP]}{K_M^G K_M^{ATP}}}{1 + \frac{[G][ATP]}{K_M^G K_M^{ATP}} + \frac{[XP][ADP]}{K_M^{XP} K_M^{ADP}}} \right) \left(1 - \frac{1}{K_{eq}^{Enz\ 1}} \frac{[XP][ADP]}{[G][ATP]} \right) \quad (10)$$

$$V^{Enz\ 2} = V_{max}^{Enz\ 2} \frac{\frac{[XP][ADP]^2[Phosphate]}{K_M^{XP}\left(K_M^{ADP}\right)^2 K_M^{Phosphate}}}{1 + \frac{[XP][ADP]^2[Phosphate]}{K_M^{XP}\left(K_M^{ADP}\right)^2 K_M^{Phosphate}} + \frac{[L][ATP]^2}{K_M^L\left(K_M^{ATP}\right)^2}} \left(1 - \frac{1}{K_{eq}^{Enz\ 2}} \frac{[L][ATP]^2}{[XP][ADP]^2[Phosphate]} \right) \quad (11)$$

$$V^{ATPase} = V_{max}^{ATPase} \frac{\frac{[ATP]}{K_M^{ATP}}}{1 + \frac{[ATP]}{K_M^{ATP}} + \frac{[Phosphate][ADP]}{K_M^{Phosphate} K_M^{ADP}}} \left(1 - \frac{1}{K_{eq}^{ATPase}} \frac{[ADP][Phosphate]}{[ATP]} \right) \quad (12)$$

We then assumed that catalytic sites are saturated with substrates and regulatory sites are saturated with regulators simplifying the rate equations to Eqs. 16, 17, and 18.

The two-enzyme model is a system of ODEs. The number of equations is equal to the number of metabolites, and each equation consists of a derivative of metabolite concentration with respect to time being equal to the sum of enzyme rates producing the metabolite minus the sum of enzyme rates consuming the metabolite:

$$\begin{aligned}
\frac{d[G]}{dt} &= 0 \\
\frac{d[XP]}{dt} &= V^{Enzyme\ 1} - V^{Enzyme\ 2} \\
\frac{d[L]}{dt} &= 0 \\
\frac{d[ATP]}{dt} &= -V^{Enzyme\ 1} + 2V^{Enzyme\ 2} - V^{ATPase} \\
\frac{d[ADP]}{dt} &= V^{Enzyme\ 1} - 2V^{Enzyme\ 2} + V^{ATPase} \\
\frac{d[Phosphate]}{dt} &= V^{ATPase} - V^{Enzyme\ 2}
\end{aligned} \quad (13)$$

Please cite this article in press as: Choe et al., Glycolysis model shows that allostery maintains high ATP and limits accumulation of intermediates, Biophysical Journal (2025), https://doi.org/10.1016/j.bpj.2025.03.037

We numerically simulated Eq. 1 using the DifferentialEquations.jl library (46) using Rodas5P solver for stiff differential equations with 10^{-15} absolute tolerance and 10^{-8} relative tolerance as for the full model described above.

RESULTS

Tasks of glycolytic ATP homeostasis

Glycolytic ATP homeostasis performs multiple tasks that likely require distinct regulation. In this section, we highlight four tasks of glycolytic ATP homeostasis that we have investigated (Fig. 1 *A*):

Task no. 1: matching the rates of ATP production and consumption. Any mismatch between the ATP consumption rate by intracellular processes and the ATP production rate by glycolysis and respiration must only be short-lived due to the ∼1–100 s turnover time of intracellular ATP (55).

Task no. 2: ensuring that ATP hydrolysis generates energy. The energy of ATP hydrolysis is set by the extent to which ATP hydrolysis reaction is maintained far from equilibrium, which, in turn, is determined by the relative levels of ATP, ADP, and inorganic phosphate. Inside the cell, ATP hydrolysis reaction is maintained 10^9- to 10^{11}-fold away from equilibrium or 20–25 k_BT of energy (55).

Task no. 3: maintaining most of the adenine nucleotide pool in the form of ATP (56,57). One function of maintaining high and stable ATP levels could be to ensure that ATP-consuming enzymes are not kinetically limited for ATP. For example, the K_M values for ATP of kinases (58), myosin (59), and Na^+/K^+-ATPase (60) are in the 1–400 μM range, indicating that these enzymes are mostly saturated with ATP given the 1–10 mM range of intracellular ATP levels. We note that we deliberately did not refer to task no. 3 by the frequently used term "energy charge of the adenylate pool" (61) to highlight that task no. 3 is unrelated to the energy of ATP hydrolysis and is distinct from task no. 2 as the ATP hydrolysis reaction can generate the same amount of energy at a wide range of ATP/ADP ratios due to the offsetting effect of inorganic phosphate.

Task no. 4: maintaining glycolytic intermediate concentration within a physiological range. Intracellular metabolite concentrations must be maintained within a finite range (62) bounded by a total intracellular concentration of molecules (<200 mM) and by the necessity of having more than one molecule of a metabolite per cell (>1 pM for a HeLa cell). Equilibrium constants of glycolytic reactions range from 10^{-6} to 10^4, making this a nontrivial task for mass action-based regulation.

In addition, glycolysis performs the tasks above at a wide range of ATP demands, responds quickly to changes in ATP demand, and coordinates its activity with branching pathways such as respiration and pentose phosphate pathway. The ability of glycolysis to perform these tasks must be robust to the physiological variability of enzyme levels, cofactor pool sizes, extracellular glucose, and lactate concentrations, as well as kinetic constants that can change with temperature or pH. Such robustness is an important property of the homeostasis (63,64). Finally, there might

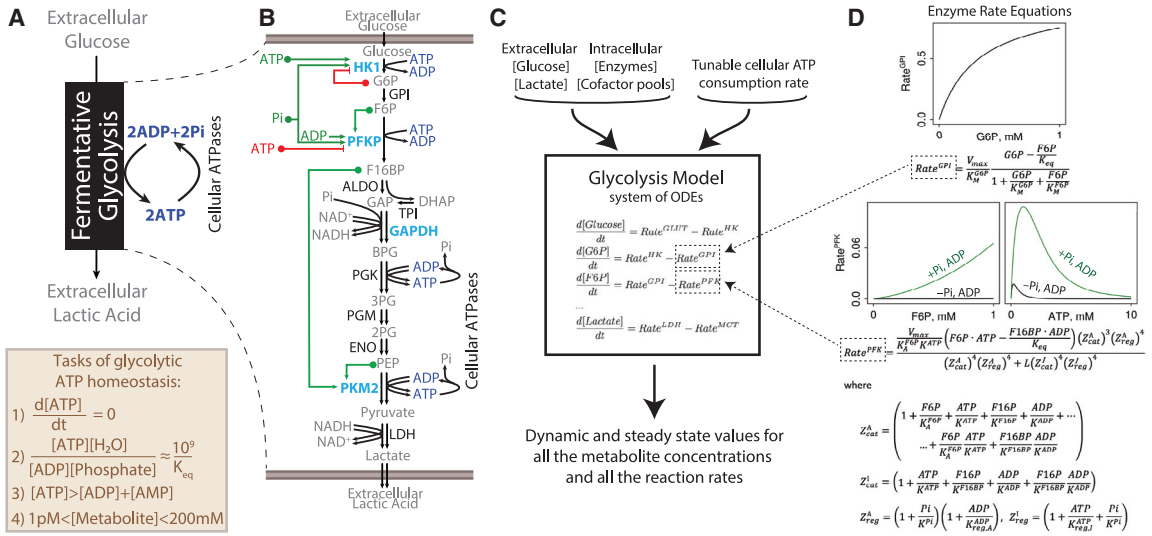

FIGURE 1 Overview of the biophysical model of mammalian glycolysis. (*A*) Coarse-grained description of aerobic glycolysis highlighting its main function to transform glucose into ATP and listing the tasks of glycolytic ATP homeostasis. (*B*) Qualitative schematic of glycolysis showing the chain of enzymes (allosterically regulated enzymes in teal and the other enzymes in black) that convert substrates into products (*gray*). Allosteric activators (*green*) and inhibitors (*red*) that are included in the model are highlighted. (*C*) Schematic of the glycolysis model, including inputs and outputs. (*D*) Kinetic rate equations are shown for GPI and PFK, and plots are actual GPI and PFK rates calculated by the respective equations with rates normalized to V_{max}. Note the dramatic allosteric activation of the PFK rate in the presence of inorganic phosphate (Pi) and ADP. See also supporting material for details on enzyme rate equation derivation.

Please cite this article in press as: Choe et al., Glycolysis model shows that allostery maintains high ATP and limits accumulation of intermediates, Biophysical Journal (2025), https://doi.org/10.1016/j.bpj.2025.03.037

be other tasks of ATP homeostasis that we are not yet aware of.

Kinetic model of glycolytic ATP homeostasis

To investigate the regulation of ATP homeostasis, we have developed a comprehensive mathematical model of mammalian glycolysis. In this section, we provide an overview of the model development while most of the technical details are described in materials and methods, as well as a comprehensive supporting material that contains all the enzyme rate derivations. Our model includes key allosteric regulators based on a thorough literature review. Most human glycolytic enzymes are encoded by several homologous genes that produce enzyme isoforms with tissue-specific expression and distinct kinetic and allosteric properties. To facilitate experimental testing, we focused on glycolytic enzyme isoforms that are most abundant in proliferating cell lines (i.e., HK1, PFKP, and PKM2 isoforms of HK, PFK, and PK) based on proteomics data (34) (see Data S1 for enzyme concentrations). We sought to develop a core model of mammalian glycolysis that supports ATP homeostasis in the absence of input from other pathways, and hence we only included allosteric regulators that are products or substrates of glycolytic enzymes. Our model converts a qualitative schematic of allosteric regulation (Fig. 1 *B*) into a precise mathematical language. As input, the model uses 1) the extracellular concentrations of glucose and lactate, 2) cellular concentrations of cofactor pools and glycolytic enzymes, and 3) the rate of cellular ATP consumption (Fig. 1 *C*). We highlight these inputs separately from the model as these inputs are not controlled by glycolysis but depend on the cell type or experimental conditions and thus cannot be predicted by a glycolysis model. The model takes these inputs and uses enzyme rate equations assembled into a system of coupled ODEs to calculate the concentration of every glycolytic intermediate and the rate of every reaction. Materials and methods contain a detailed description of the model, including ODE equations, stoichiometric matrix, ODE solvers, conserved moieties, simulation setting, etc. Our model can calculate both steady-state behavior and dynamical responses to perturbations. In effect, our model uses in vitro enzyme kinetics to predict any measurable property of glycolysis and many properties that cannot currently be measured.

In total, our model contains 172 parameters, including kinetic and thermodynamic constants and estimates of enzyme and cofactor pool concentrations, yet all these parameters are tightly constrained by experimental data. Kinetic constants were estimated from in vitro enzyme kinetics data (Data S2) as described briefly below and in full detail in supporting material. Thermodynamic constants are taken from the eQuilibrator database (65). Enzyme and cofactor pool concentrations are estimated from proteomics and metabolomics data, respectively, as described in materials and methods and reported in Data S1. We numerically simulate the model using the DifferentialEquations.jl library (46) written in the Julia Programming Language (66). Our code is heavily optimized so that it takes ∼10 ms to calculate the results of the model under given conditions using a single core of a modern computer processor. Optimized code allows us to run the model under millions of different conditions to systematically explore the regulation of glycolytic ATP homeostasis.

The defining feature of our model is the use of newly derived kinetic rate equations to describe the activity of four allosterically regulated enzymes (i.e., HK1, PFKP, GAPDH, PKM2) using the MWC model. MWC is a powerful model for describing the activity of allosterically regulated enzymes (9–11,32,33), which assumes that allosteric enzymes exist in two or more conformations with different kinetic properties. Both the binding of substrates and allosteric regulators can modify the kinetic properties of an MWC enzyme by stabilizing one conformation over another. We use statistical learning approaches—regularization and cross-validation—to identify the simplest MWC kinetic rate equation that adequately describes the available in vitro kinetic data, allowing us to avoid overfitting and parameter identifiability issues common for fitting complex equations to finite data (67). The MWC equation describing the rate of PFKP in the presence of substrates and regulators is shown in Fig. 1 *D*. We described nonallosterically regulated glycolytic enzymes (*black* in Fig. 1 *B*) using standard kinetic rate equations derived from quasisteady-state or rapid equilibrium approximations. For the eight enzymes and transporters with one substrate and one product and for aldolase (ALDO) with two products, we used reversible Michaelis-Menten equations (see equation describing the rate of glucose-6-phosphate isomerase [GPI] in Fig. 1 *D*) and sequential release equation for ALDO, respectively, and estimated their kinetic constants by averaging the values from at least three publications per constant to verify their consistency and accuracy. For the two remaining enzymes with more than one substrate or product—phosphoglycerate kinase (PGK) and lactate dehydrogenase (LDH)—we fitted their more complex rate equations to manually curated in vitro kinetics datasets containing 350–700 data points per enzyme (Data S2). We chose to fit data for PGK and LDH instead of averaging over published kinetic constants because many publications describing PGK and LDH activity used different rate equations, and hence the published kinetic constants are not directly comparable. A comprehensive description of the derivations and fitting of all the enzyme rate equations is reported in supporting material and in vitro kinetic data is compiled in Data S2, and we hope this compendium of information will serve as a great resource for future investigations of these enzymes.

Our model uses several assumptions that must be considered when interpreting its predictions. First, the model assumes that the activity of enzymes in living cells is accurately described using in vitro activity of purified enzymes. Second, the model assumes that enzymes and

Please cite this article in press as: Choe et al., Glycolysis model shows that allostery maintains high ATP and limits accumulation of intermediates, Biophysical Journal (2025), https://doi.org/10.1016/j.bpj.2025.03.037

metabolites are well mixed in the cytosol of the cell. Third, the model only describes the effect of regulators that are included in the model. Fourth, the model assumes that other pathways (e.g., pentose phosphate pathway, mitochondrial pyruvate consumption) do not affect the concentration of glycolytic intermediates or glycolytic reaction rates. Finally, the model does not consider the effect of glycolysis on pH and the resulting modification of enzyme activity. Deviations between the model and experimental observations could be due to any number of these assumptions not being valid under the conditions of a particular experiment. On the other hand, if the model accurately predicts experimental data, it suggests that these assumptions are valid under given experimental conditions.

Glycolysis model robustly performs the key tasks of glycolytic ATP homeostasis

After constructing the model, we first performed simulations to determine whether the glycolysis model can perform the key tasks of ATP homeostasis described above (Fig. 1 *A*). To simulate ATP consumption by intracellular processes, we included an ATPase enzyme in the model. Glycolysis cannot proceed faster than the maximal rate of its slowest enzyme, so we report all ATPase rates in percent of the maximal activity of HK1—the slowest enzyme of glycolysis based on the product of intracellular enzyme concentration and V_{max}. First, we found that the glycolysis model produces as much ATP as is consumed and rapidly adjusts to stepwise increase or decrease of ATP consumption, as is necessary under physiological conditions (Fig. 2 *A*). Second, we showed that $>>90\%$ of the adenine nucleotide pool was maintained as ATP and ATP concentrations varied by $<<10\%$ when we introduced physiologically relevant twofold stepwise changes in ATP consumption rate (Fig. 2 *B*). Thus, as has been observed in vivo (56,57), our model maintains nearly constant ATP levels in response to large changes in ATP turnover. Finally, we showed that the glycolysis model maintains ATP, ADP, and inorganic phosphate concentrations such that the ATP hydrolysis reaction is $\sim 10^9$-fold away from equilibrium, equivalent to ~20–25 k_BT (Fig. 2 *C*), which is similar to what has been measured in cells (55).

We next tested whether the ability of the model to perform the relevant tasks of ATP homeostasis is robust to changes in glycolytic enzyme levels that are variable from cell to cell and to uncertainty in our estimates of biochemical constants, cofactor pool concentrations, and initial concentrations of intermediates. To demonstrate robustness, we reran our model 10,000 times using random values of enzyme levels taken from a log-uniform distribution spanning a ninefold range around the model estimates based on proteomics data (Fig. S1, *A–C*) as well as random values of model parameters (Fig. S1, *D–F*) and initial condition value (Fig. S1, *G–K*) taken from a normal distribution with mean and standard error corresponding to experimental estimates of corresponding values (see Data S1 for model estimates on enzyme levels and initial conditions and supporting material for mean and standard error of kinetic constants). Our simulations showed that 95% confidence intervals of model prediction are largely independent of glycolytic enzyme levels, model parameters, and initial conditions, as would be expected for the model that captures the robust endogenous regulatory circuit of glycolytic ATP homeostasis.

Glycolysis model predicts several metrics of glycolysis activity that are consistent with measurements in proliferating mammalian cell lines

Given that our model could reproduce the wealth of measurements of each glycolytic enzyme in vitro and perform the key tasks of ATP homeostasis, we set out to evaluate how the model's predictions compare to the results of experiments in proliferating mammalian cell lines.

First, we briefly discuss our expectations for comparing model predictions and data, given the many differences between the model and living cells. The model is based on in vitro kinetic measurements and focuses solely on the glycolysis pathway, so we do not expect that the model predictions will perfectly align with cellular measurements due to different conditions in vitro and within cells, as well as the presence of additional metabolic pathways branching off from glycolysis. However, given that the model robustly maintains ATP homeostasis at a wide range of parameter values (Figs. 2, *A–C* and S1) and glycolysis is the most active metabolic pathway in proliferating mammalian cells, we expect the predictions to agree with experimental data within an order of magnitude. Specifically, we will consider the model predictions to be consistent with the measurements when the 95% confidence intervals of the predictions and experimental measurements overlap.

We first compared the range of glycolytic fluxes where the model supports the tasks of ATP homeostasis to the range of glycolytic fluxes measured in proliferating mammalian cells. The model could support a range of glycolytic rates ~0.0003–0.010 μmol glucose/min/mg cellular protein (Fig. 2 *D*), which overlaps with glycolytic flux measurements from two dozen proliferating cells (68). Several cell lines exhibit higher glycolytic fluxes than our model can support. The latter is likely driven by higher glycolytic enzyme expression in those cell lines, as we have observed a 10-fold range of HK expression in proteomics data (see Fig. 6, *A* and *B* below).

We next compared the model predictions with measurements of absolute intracellular metabolite concentrations. To test if our model can recapitulate the vast range of glycolytic activities seen in prior experiments, we not only compiled data from nine publications analyzing whole-cell absolute intracellular glycolytic intermediate concentrations

Please cite this article in press as: Choe et al., Glycolysis model shows that allostery maintains high ATP and limits accumulation of intermediates, Biophysical Journal (2025), https://doi.org/10.1016/j.bpj.2025.03.037

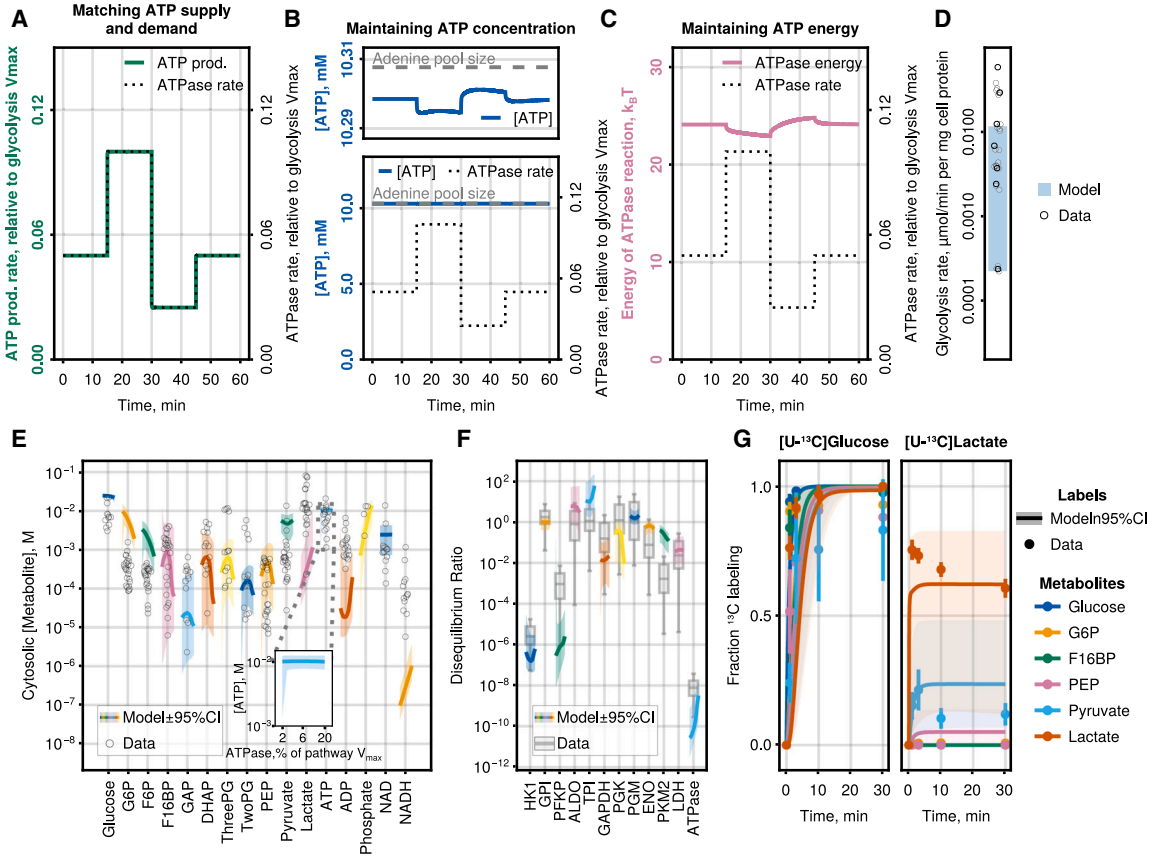

FIGURE 2 Glycolysis model recapitulates glycolysis activity observed in live cells. (*A–C*) Model simulations showing changes in (*A*) ATP production rate, (*B*) ATP concentration (total adenine pool size is labeled with a *dashed gray line*), and (*C*) energy released during ATP hydrolysis in response to a twofold stepwise increase or decrease of ATPase rate. Starting ATPase rate = 5% of glycolysis V_{max} was used for (*A*)–(*C*). ATPase energy is calculated as a natural logarithm of the disequilibrium ratio for the ATPase reaction (i.e., mass-action ratio divided by the equilibrium constant) for the ATPase reaction. (*D*) Range of glycolysis rates supported by the model (*blue shaded area*) compared with rates measured in living cells (*open circles*). (*E*) Comparison of model predictions with measured glycolytic intermediate concentrations from multiple cell lines and experimental conditions. Black empty circles indicate the experimentally determined metabolite concentrations. Colored lines with ribbon indicate the median and 95% CI of model predictions. The shift from left to right for each metabolite level prediction corresponds to increasing rates of ATP consumption from 2 to 20% of glycolysis V_{max} (see *inset* for ATP) to highlight the effect of ATP consumption on metabolite concentrations. Note that data points are displayed with pseudorandom jitter and do not have shifts corresponding to ATP consumption rate. Model predictions represent the concentration of bound + free metabolites in the whole-cell analogous to whole-cell metabolite measurements, while in all other figures, model output is the free concentration of metabolites in the cytosol. (*F*) Comparison of model predictions with disequilibrium ratios (i.e., ratio of mass action balance to equilibrium constant) for each glycolysis reaction estimated using the experimental estimates. The range of experimental disequilibrium ratios displayed in the box and whiskers plot is calculated using 1000 bootstraps of metabolite concentration values from (E). Whiskers are 1.5 times interquartile range. (*G*) Comparison of model prediction with [U-$^{13}C_6$]glucose and [U-$^{13}C_3$]lactate tracing data averaged for C2C12 and HeLa cells. Points are data (*error bars* are SD), and lines are model predictions (*ribbons* are 95% CI). ATPase rate = 15% of glycolysis V_{max} was chosen for model predictions. Model predictions in (*D*) and (*E*) are from simulations where bootstrapped model parameter combinations could match ATP supply and demand, which were >97 and >95% of simulations for (*E* and *F*) and (*G*), respectively. See also Fig. S1. Julia code to reproduce this figure is available at https://github.com/DenisTitovLab/CellMetabolism.jl.

using LC-MS, but also supplemented these data with our measurements in four cell lines (see Data S1). Our model predicts free metabolite concentration in the cytosol, while LC-MS measures the sum of free and enzyme-bound metabolite concentrations in whole cells. To directly compare model predictions to data from bulk cell measurements, we adjusted the model predictions to report the sum of enzyme-bound and free metabolite concentration and the whole-cell measurements to report cytosolic metabolite concentrations (see materials and methods for additional details of the adjustments). In addition, we reported model predictions at a range of cellular ATP demands observed in proliferating cell lines (see Fig. 2 *D*), as the corresponding ATP demand was not measured for most of the LC-MS data. We observed that 95% confidence intervals of model predictions of most of the glycolytic intermediate concentrations overlapped with experimental measurements (Fig. 2 *E*). The latter result is notable given that our model contains no direct information about intracellular metabolite levels and is free to predict concentrations from 0 to $+\infty$ and even below zero if the model is implemented incorrectly. The only metabolite where confidence intervals of

Please cite this article in press as: Choe et al., Glycolysis model shows that allostery maintains high ATP and limits accumulation of intermediates, Biophysical Journal (2025), https://doi.org/10.1016/j.bpj.2025.03.037

model predictions do not overlap with experimental values is NADH. A large fraction of cellular NADH is inside of mitochondria (69) and most of the intracellular NADH exists in protein-bound form in complex with various dehydrogenases (69). Mitochondria and nonglycolytic dehydrogenases are not included in our model, which might explain the discrepancy in predicted NADH levels and experiments. The NAD^+/NADH ratio of ~1000 predicted by the model at high ATP demand is similar to estimates of ~1000 for cytosolic NAD^+/NADH ratios (69,70). The model also tends to predict higher average levels of G6P, F6P, and pyruvate and lower average levels of lactate and ADP than corresponding experimental values.

Another way to compare model prediction and metabolite levels is to look at the disequilibrium ratios of each glycolytic reaction. The disequilibrium ratio ρ denotes the reaction's distance from equilibrium and is calculated using the ratio of mass action ratio and equilibrium constant:

$$\rho = \frac{1}{K_{eq}} \frac{\prod_i [Product_i]}{\prod_i [Substrate_i]} \quad (14)$$

The 95% confidence interval of model predictions of disequilibrium ratios overlaps with experimental estimates for most glycolytic reactions (Fig. 2 *F*). The main quantitative differences are that the model predicts PFKP to be further away from equilibrium and PKM2 closer to equilibrium than is observed in the data.

Next, we compared [U-$^{13}C_6$]glucose- and [U-$^{13}C_3$]lactate-labeling kinetics predicted by the model to cellular measurements. For these measurements, we exchanged normal media for media containing [U-$^{13}C_6$]glucose or [U-$^{13}C_3$]lactate and then lysed cells at different time intervals to estimate the rate and fraction at which ^{13}C from [U-$^{13}C_6$]glucose or [U-$^{13}C_3$]lactate is incorporated into glycolytic intermediates. Once again, we observed that the 95% confidence intervals of glycolysis model prediction overlapped with the measurements of the ^{13}C labeling fraction of intermediates after switching to [U-$^{13}C_6$]glucose- or [U-$^{13}C_3$]lactate-containing media (Fig. 2 *G*). It is noteworthy that the model can recapitulate labeling from [U-$^{13}C_3$]lactate where only intracellular lactate and pyruvate are labeled. The ^{13}C label from [U-$^{13}C_3$]lactate can propagate in the opposite direction of the net flux using reaction reversibility. Our experimental data and model predictions show that the ^{13}C label from [U-$^{13}C_3$]lactate appears only in intracellular lactate and pyruvate, indicating that the lactate transporter (MCT) and LDH—but not PK—are near equilibrium and, thus, highly reversible. The agreement between model predictions and experimental results validates the model's ability to quantify reaction reversibility within this segment of the glycolytic pathway. The main quantitative difference between ^{13}C-labeling experiments and model predictions is that the model predicts slower average labeling kinetics from [U-$^{13}C_6$]glucose for metabolites starting with G6P but not glucose.

In summary, our model predicts several orthogonal measurements of glycolysis activity that are consistent with measurements in living cells. To the best of our knowledge, this is the first example of a biophysical model of mammalian glycolysis based exclusively on in vitro enzyme kinetic data that are capable of accurately predicting various estimates of glycolysis activity in living cells.

Allosteric regulation is required to maintain high ATP levels while mass action performs other tasks of glycolytic ATP homeostasis

Having established that the model recapitulates the key tasks of ATP homeostasis and makes predictions that are consistent with measurements in proliferating mammalian cells, we next used the model to investigate the function of allosteric regulation and mass action in maintaining ATP homeostasis.

We first removed all allosteric regulators to see if the resulting pathway remained functional. Specifically, we made the HK1, PFKP, GAPDH, and PKM2 enzymes behave as Michaelis-Menten-like enzymes with kinetic parameters corresponding to their active MWC conformation. We also removed inhibition of the HK catalytic site by G6P, which proceeds through standard nonallosteric competitive inhibition. Surprisingly, the model without allosteric feedback could match ATP supply and demand and maintain the high energy of ATP hydrolysis with only minor quantitative differences compared with the model with allostery (Fig. 3, *A–D* and *F*). However, we observed a complete breakdown of high ATP level maintenance without allosteric regulation, where ATP levels were >100-fold lower, and a small 2-fold increase and decrease in ATPase rate led to an almost 10-fold change in ATP concentration compared with <<10% change in ATP concentration for the complete model (Fig. 3, *B* and *E*). Systematic investigation of steady-state model behavior at different ATPase rates showed that the model without allosteric feedback is not capable of maintaining most of the adenine nucleotide pool in the form of ATP at any ATPase rate, which is contrary to the constant ATP concentrations observed both in vivo (56,57) and in the model with allosteric feedback (Fig. 3 *E*, vertical drop-off indicates where the ATP production by the model cannot match ATPase rate anymore). Beyond ATP, removing allostery caused dramatic shifts in levels of most glycolytic intermediates (Fig. S2). Metabolites significantly affected by the removal of allosteric regulation—such as F6P, G6P, F16BP, 3PG, 2PG, PEP, ATP, and phosphate—deviated further from experimental values than the model with allostery, providing additional evidence that our model accurately captures glycolytic regulation, including allosteric interactions (Fig. S2). Finally, we note

Please cite this article in press as: Choe et al., Glycolysis model shows that allostery maintains high ATP and limits accumulation of intermediates, Biophysical Journal (2025), https://doi.org/10.1016/j.bpj.2025.03.037

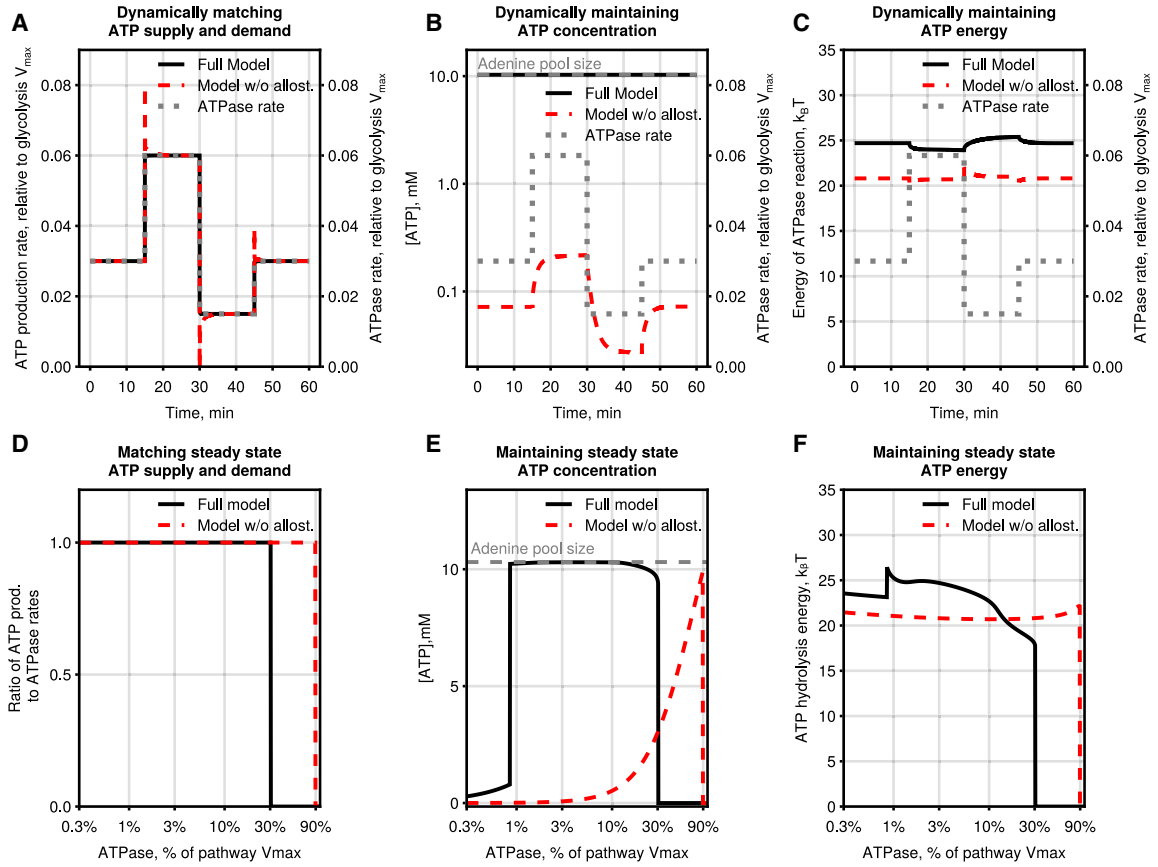

FIGURE 3 Allosteric regulation is required for the maintenance of high ATP levels. (*A*–*C*) Model simulations showing the effect of removal of allosteric regulation of HK1, PFKP, GAPDH, and PKM2 on dynamic changes in (*A*) ATP production rate, (*B*) ATP concentration, and (*C*) energy released during ATP hydrolysis (left axes) in response to a twofold stepwise increase or decrease of ATPase rate (right axes). Starting ATPase rate = 3% of glycolysis V_{max} was used for (*A*)–(*C*). Energy is calculated as a natural logarithm of the disequilibrium ratio (i.e., mass-action ratio divided by the equilibrium constant) for the ATPase reaction. (*D*–*F*) Model simulations showing the effect of removal of allosteric regulation of HK1, PFKP, GAPDH, and PKM2 on steady-state (*D*) ATP production rate, (*E*) ATP concentration, and (*F*) energy released during ATP hydrolysis at a 100-fold range of ATPase rates. Dashed gray lines in (*B*) and (*E*) indicate the total adenine pool size (i.e., ATP + ADP + AMP). See also Figs. S2 and S3. Julia code to reproduce this figure is available at https://github.com/DenisTitovLab/CellMetabolism.jl.

that the full model fails to maintain most of the adenine pool in the form of ATP at high ATPase rate—an expected consequence of ATPase rate being higher than the maximal activity of glycolytic enzymes—and low ATPase rate—an unexpected observation that we will explore below as it connects to the function of allosteric regulation of glycolysis (Fig. 3 *E*, vertical drop-offs at high and low ATPase rates).

Comparison of the model to published glycolysis models

Several kinetics models of glycolysis have been reported over the past several decades (28–31), yet none of these reports investigated whether those models can recapitulate the tasks of ATP homeostasis that we identified (Fig. 1 *A*). Most of the published models either did not include ATP, ADP, or Pi or kept them constant, making it difficult to investigate ATP homeostasis using those models. We performed head-to-head comparisons of our model with three mechanistic models of glycolysis that we will refer to as the Mulquiney model (29), the van Heerden model (30), and the Shestov model (31). To the best of our knowledge, these are the only three mechanistic models of glycolysis that use in vitro enzyme kinetics and include variable ATP, ADP, and Pi. However, even in these models, Pi levels are linked to extracellular or vacuolar pools with rapid reactions, rendering them practically constant. Mulquiney and Shestov models simulate mammalian glycolysis and the van Heerden model simulates *S. cerevisiae* glycolysis. All three models incorporate allosteric regulation of HK, PFK, and PK enzymes, but each model only contains a subset of allosteric regulators included in our model, and none of the models were previously used to investigate the function of allosteric regulation of glycolysis. We repeated the simulations in Fig. 3, *D*–*F* using the kinetic rate equations for glycolytic enzymes from the Mulquiney, Shestov, and van Heerden models (Fig. S3). All three models could match ATP supply and demand and maintain the high energy of

Please cite this article in press as: Choe et al., Glycolysis model shows that allostery maintains high ATP and limits accumulation of intermediates, Biophysical Journal (2025), https://doi.org/10.1016/j.bpj.2025.03.037

ATP hydrolysis (Fig. S3, *A*, *C*, *D*, *F*, *G*, and *I*). Note that the Mulquiney, van Heerden, and our model could match ATP supply and demand at similar ATPase rates up to about 10–30% of the respective pathway V_{max}, while the Shestov model could only support much lower ATPase rates up to 0.003% of its V_{max}. The Mulquiney and Shestov models could maintain most of the adenine pool in the form of ATP at a 2.8- and 2.2-fold range of ATPase values compared with a 38-fold range for our model, while the van Heerden model could not maintain high ATP under any ATPase rates (Fig. S3, *B*, *E*, and *H*). The ability of our model to maintain high ATP levels at a wider range of ATPase rates compared with these published models is likely the result of incorporating more allosteric regulators and fitting MWC rate equation to kinetic data from multiple publications. Importantly, as for our model, the Mulquiney and Shestov models maintained high ATP levels only in the presence of allosteric feedback (Fig. S3, *B*, *E*, and *H*). Comparison with previously published models further confirms our observations that the maintenance of high ATP levels requires allosteric regulation. In contrast, mass action is sufficient for glycolysis to match ATP supply and demand and maintain the high energy of ATP hydrolysis.

Redundant allosteric regulators of HK1 and PFKP maintain high and stable ATP levels

To identify the role of specific allosteric regulators in maintaining high and stable ATP levels, we computationally dissected the pathway by removing the allosteric regulation of enzymes one by one (Fig. 4). Specifically, we removed a particular allosteric regulator from the relevant kinetic rate equations by setting its binding constant for both active and inactive MWC conformation to ∞ and setting the constant *L* that determines the ratio of inactive to active MWC conformations to zero. We found that the allosteric regulation of HK1 and PFKP is responsible for maintaining high and stable ATP levels, whereas removing the allosteric

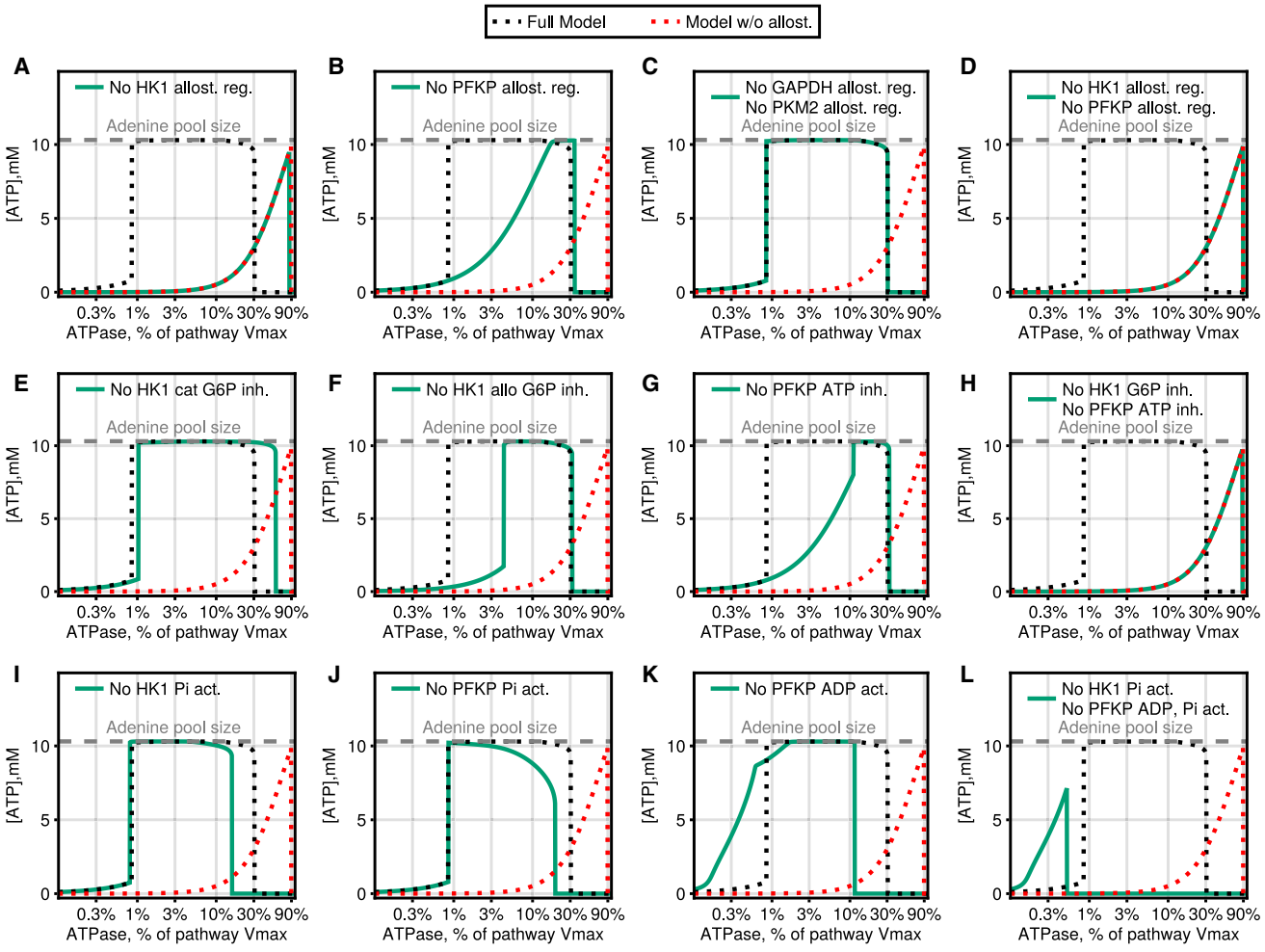

FIGURE 4 Redundant allosteric regulators of HK and PFK are required to maintain high ATP levels. (*A–L*) Steady-state ATP concentrations at a range of ATPase rates of the glycolysis model with and without (*A–D*) allosteric regulation of enzymes, (*E–H*) allosteric inhibitors, and (*I–L*) allosteric activators. Dashed gray line indicates the total adenine pool size (i.e., ATP + ADP + AMP). See also Fig. S4. Julia code to reproduce this figure is available at https://github.com/DenisTitovLab/CellMetabolism.jl.

Please cite this article in press as: Choe et al., Glycolysis model shows that allostery maintains high ATP and limits accumulation of intermediates, Biophysical Journal (2025), https://doi.org/10.1016/j.bpj.2025.03.037

regulation of GAPDH and PKM2 had no discernable effect (Fig. 4, *A–D*). Digging further, we removed each of the allosteric activators and inhibitors of HK1 and PFKP and found that these regulators work together to ensure the robust maintenance of ATP levels since removing any single regulator only led to a partial loss of ATP maintenance capacity. In general, removing inhibitors—G6P for HK1 and ATP for PFKP—led to worse ATP maintenance at low ATPase rates (Fig. 4, *E–H*), while removing activators—phosphate for both HK1 and PFKP and ADP for PFKP—led to poorer ATP maintenance at high ATPase rates (Fig. 4, *I–L*).

Global sensitivity analysis of the model confirms the role of allostery in maintaining high ATP levels

We next performed a global sensitivity analysis of our model to systematically explore the role of all model parameters in matching ATP supply and demand, maintaining high ATP levels, and maintaining high energy of ATP hydrolysis. The goal of global sensitivity analysis is to estimate the contribution of each model parameter and parameter interactions to the variance of a specific model output (50). Global sensitivity analysis is conceptually similar to a local sensitivity analysis technique called metabolic control analysis (48,49), but is more powerful as it allows for interaction between model parameters and investigates the global model behavior at any range of parameter values as opposed to local model behavior at infinitely small changes around a specific parameter value. We used the average ratio of ATP production to ATP consumption, average ratio of ATP concentration to adenine pool size, and average energy of ATP hydrolysis at a log range of ATPase values as proxies for the model's ability to match ATP supply and demand, maintain high ATP levels, and maintain high energy of ATP hydrolysis, respectively. We first estimated the variance of the proxies by randomly varying each parameter of the model independently from a log-uniform distribution spanning a ninefold range from three times lower to three times higher than its value in the model. The coefficient of variation for all three proxies was in the narrow range of 0.15–0.34 in response to random changes in parameter values spanning ninefold, indicating that these are robust properties of the model (Fig. S4, *A–C*). The coefficient of variation for maintaining high ATP levels was about twofold higher than for maintaining high energy of ATP hydrolysis or for matching ATP supply and demand, suggesting that the former is more sensitive to changes in specific enzyme kinetic parameters as would be expected for a task that depends on allosteric regulation and not just mass action. Two metrics for each model parameter are typically reported for variance-based global sensitivity analysis. The first-order effect sensitivity index S_1 reports the fraction of variance of the model output that will be removed if the corresponding parameter is fixed. The total-order sensitivity index S_T reports the variance that will be left if values of all other parameters are fixed. Larger values of S_1 and S_T indicate that a given parameter is important. Global sensitivity analysis showed that kinetic parameters for HK1, PFKP, and GAPDH had the highest S_1 and S_T for all three model outputs. We subdivided kinetic parameters for HK1 and PFK into allosteric parameters that are different for active and inactive states of the enzyme and nonallosteric parameters. Nonallosteric kinetic parameters of HK1 and PFKP had the highest S_1 and S_T for matching ATP supply in demand (Fig. S4 *D*), as would be expected, given that HK1 and PFK are the slowest enzymes in the pathway, while allosteric parameters of HK1 and PFKP had the highest S_1 and S_T for maintaining high ATP levels (Fig. S4 *E*). Kinetic parameters for GAPDH had the highest S_1 and S_T for maintaining the energy of ATP hydrolysis, suggesting a role for GAPDH in the latter (Fig. S4 *F*). Thus, global sensitivity analysis confirmed the importance of allosteric regulation of HK1 and PFKP in maintaining high ATP levels, as shown in Fig. 3.

Allosteric regulation maintains high ATP levels and prevents uncontrolled accumulation of phosphorylated intermediates by inhibiting the reaction of Harden and Young

We next investigated the mechanism that allows allosteric regulators of HK1 and PFKP to maintain high and stable ATP levels. Here, we first describe the side reaction that prevents the mass action-driven glycolysis pathway from maintaining high ATP levels and then explain how allosteric regulation inhibits this side reaction. Glycolysis has an unusual organization where upper glycolysis enzymes—from HK1 to ALDO—consume ATP, while lower glycolysis enzymes—from GAPDH to LDH—consume inorganic phosphate and produce ATP. Such an organization leads to the reaction of Harden and Young (18,19,71), where two molecules of ATP produced by the conversion of glucose to lactic acid are used to phosphorylate another molecule of glucose without a net change in ATP levels (Fig. 5 *A*). The net reaction of Harden and Young is:

$$2Glucose + 2Phosphate \rightleftarrows F16BP + 2Lactic\ acid + 2H_2O \quad (15)$$

As the name suggests, the analogous reaction from yeast alcohol fermentation producing ethanol and carbon dioxide instead of lactic acid was first observed by Harden and Young in 1906 in cell-free yeast extracts (18), which predates the discovery of the physiological ATP-producing reaction of glycolysis by several decades. The reaction of Harden and Young is extremely thermodynamically favorable with an estimated $K_{eq} \approx 3 \cdot 10^{30}$ and $\Delta_r G'^{\circ} \approx -170$ kJ/mol (65), resulting in the sequestration of inorganic phosphate in phosphorylated intermediates of upper glycolysis. Importantly, as the reaction of Harden and Young does not involve net consumption or production of ATP, it will occur as long as

Please cite this article in press as: Choe et al., Glycolysis model shows that allostery maintains high ATP and limits accumulation of intermediates, Biophysical Journal (2025), https://doi.org/10.1016/j.bpj.2025.03.037

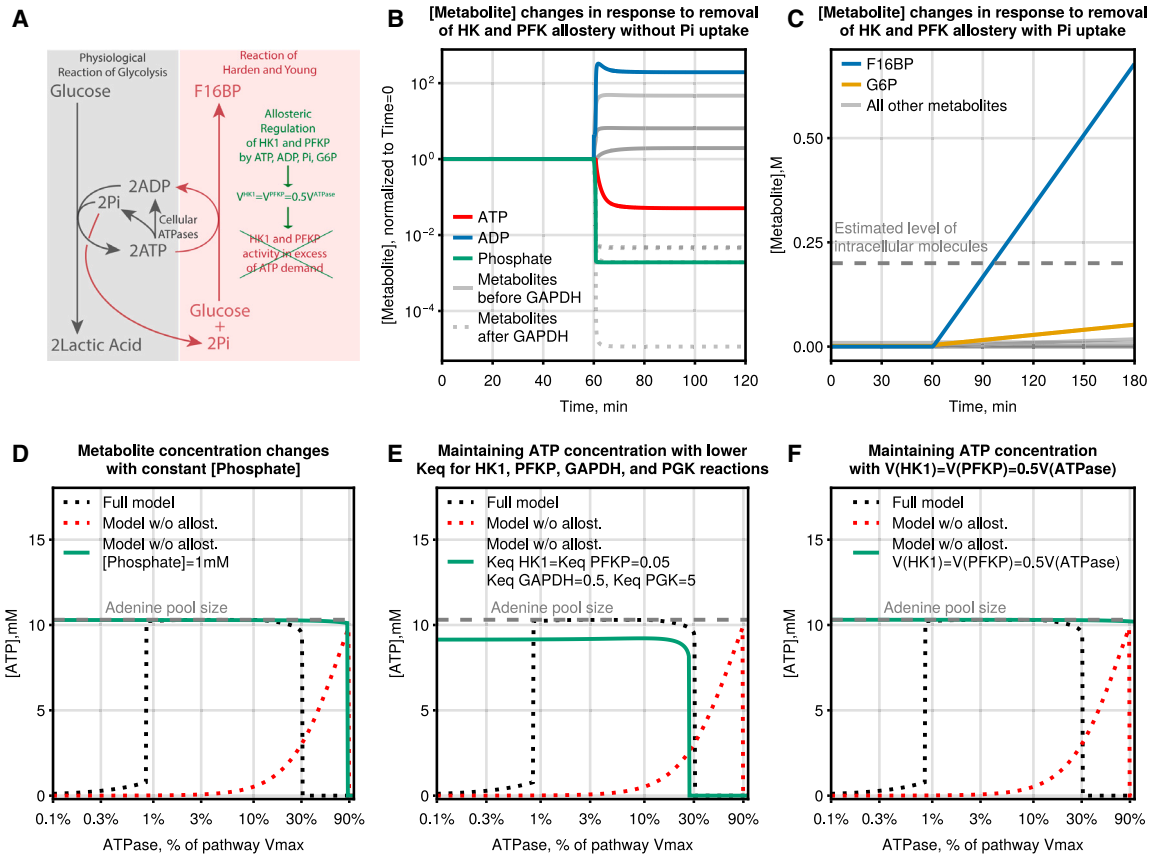

FIGURE 5 Allosteric regulation of HK and PFK maintains ATP levels and prevents accumulation of intermediates by inhibiting the reaction of Harden and Young. (*A*) Schematic of the reaction of Harden and Young and its inhibition by allosteric feedback control of HK1 and PFKP. (*B* and *C*) Phosphorylated metabolite level changes upon an instantaneous removal of allostery at 30 min in the (*B*) absence and (*C*) presence of cellular phosphate uptake. ATPase rate = 10% of glycolysis V_{max} was used for model predictions. (*D–F*) Steady-state ATP concentrations at a range of ATPase rate of the glycolysis model with (*D*) constant [phosphate] = 1 mM, (*E*) $K_{eq}^{HK1} = 0.05$ (model value 2700), $K_{eq}^{PFKP} = 0.05$ (model value 760), $K_{eq}^{GAPDH} = 0.5$ (model value 16), and $K_{eq}^{PGK} = 5$ (model value 2000), (*F*) Rate equations for HK1 and PFKP substituted for one-half of ATPase rate equations. Julia code to reproduce this figure is available at https://github.com/DenisTitovLab/CellMetabolism.jl.

glucose uptake and phosphorylation are not regulated. In the presence of exogenous glucose and phosphate uptake (e.g., uptake from the extracellular media), the reaction of Harden and Young causes uncontrolled accumulation of phosphorylated intermediates of upper glycolysis to >>200 mM concentrations that will explode cells. In the presence of glucose uptake but not phosphate uptake, this reaction causes low levels of ATP, as all the inorganic phosphate produced from ATP hydrolysis is trapped in phosphorylated intermediates of upper glycolysis at the expense of ATP levels.

We propose that the function of allosteric regulation of HK1 and PFKP is to inhibit the reaction of Harden and Young by restricting the rates of HK1 and PFKP reactions to half of the ATPase rate. The latter prevents the reaction of Harden and Young from occurring due to the lack of excess HK1 and PFKP capacity necessary to catalyze this side reaction (Fig. 5 *A*). We performed simulations to support the role of allostery in inhibiting the reaction of Harden and Young. Removal of allosteric regulation of HK1 and PFKP in the absence of cellular phosphate uptake leads to upregulation of phosphorylated metabolites upstream of the GAPDH reaction except for phosphate and downregulation of phosphorylated metabolites downstream of the GAPDH reaction, showing that the disappearance of inorganic phosphate blocks the GAPDH step in the absence of allosteric control of HK1 and PFKP (Fig. 5 *B*). Removal of allosteric regulation of HK1 and PFKP in the presence of constant phosphate levels (e.g., through uptake across plasma membrane) leads to continuous accumulation of F16BP due to the reaction of Harden and Young (Fig. 5 *C*). The level of F16BP quickly increases past 200 mM—the estimate of total small molecule concentration in a cell—and its continued accumulation will eventually explode cells. Constant levels of inorganic phosphate abrogated the requirement for allostery to maintain ATP levels, showing that allostery maintains ATP levels by preventing the disappearance of phosphate due to the reaction of Harden and Young (Fig. 5 *D*). A large decrease in equilibrium constants of HK1, PFKP, GAPDH, and PGK that makes the reaction of Harden

Please cite this article in press as: Choe et al., Glycolysis model shows that allostery maintains high ATP and limits accumulation of intermediates, Biophysical Journal (2025), https://doi.org/10.1016/j.bpj.2025.03.037

and Young less thermodynamically favorable also removed the requirement for allostery for high ATP maintenance (Fig. 5 *E*). Finally, directly making the HK1 and PFKP rates equal to one-half of the ATPase rate abolished the requirement for allostery for both high ATP maintenance and uncontrolled accumulation of F16BP, suggesting that allostery works by tying HK1 and PFKP rates to the ATPase rate (Fig. 5 *F*).

The described function of allosteric regulation of HK and PFK explains why the model predicts a collapse at low ATPase rates (Fig. 3 *E*, vertical drop-off of ATP level at ATPase rates of ∼1% pathway V_{max}). According to the proposed function, when ATP consumption is near zero, allosteric feedback must reduce HK and PFK activity to nearly zero. However, completely stopping HK and PFK reactions is not feasible as it would require infinite levels of allosteric inhibitors. Thus, allosteric regulation can only inhibit the reaction of Harden and Young within certain upper and lower limits of ATP consumption rates. This theoretical prediction is supported by experimental observations (19,71) showing that the reaction of Harden and Young is observed in yeast extracts in the absence of ATPase but not in the presence of ATPase, in agreement with simulations in Fig. 3 *E*.

Extensive published experimental evidence supports the existence of the reaction of Harden and Young, as discussed further in the discussion.

Excess activity of glycolytic enzymes relative to HK and PFK is required to maintain high ATP levels

We next explored whether attributes of the glycolysis pathway other than allosteric regulation of HK1 and PFKP might be required for maintaining most of the adenine pool in the form of ATP. During model construction, we noted that proteomics data show that most mammalian glycolytic enzymes are expressed in large excess compared with HK1, PFKP, glucose transporter, and lactate transporter (Fig. 6 *A*). After accounting for the specific activity of enzymes, the maximal cellular activity of most enzymes is 10- to 100-fold higher than is required for the maximal activity of the glycolysis pathway that is limited by HK1 (Fig. 6 *B*). Allosteric inhibition of HK1 and PFKP by G6P and ATP, respectively, further increases the differential between the activity of HK1 and PFKP and the rest of the enzymes. We used our model to understand the rationale for this seemingly wasteful enzyme expression pattern, given that the production of excess glycolytic enzymes represents a significant investment of resources by the cell, with enzymes such as GAPDH and PKM2 approaching 1% of the proteome. Increasing the concentrations of enzymes from TPI to LDH by 10-fold led to no changes in ATP maintenance (Fig. 6 *C*). Decreasing the concentrations of these enzymes by 10- and 50-fold led to a small decrease and complete collapse of ATP level maintenance, respectively, with <2-fold effect on the ability of the model to produce ATP (Fig. 6 *C*). We propose that the high expression of glycolytic enzymes in relation to HK1 and PFKP works together with allosteric regulation to inhibit the reaction of Harden and Young by ensuring that HK1 and PFKP remain far from equilibrium. The reasoning behind this is that if another enzyme matches the activity of HK or PFK in the presence of allosteric effectors, the HK and PFK reactions cannot remain far from equilibrium, causing the reaction of Harden and Young to resume operating. Our results provide a mechanistic explanation for the seemingly wasteful large excess expression of glycolysis enzymes relative to HK1 and PFKP.

Coarse-grained model of glycolysis recapitulates key tasks of ATP homeostasis

To gain a better understanding of the tasks of ATP homeostasis that can be achieved by mass action alone and which might require allostery, we used a simplified model of glycolysis, referred to as the two-enzyme model, containing

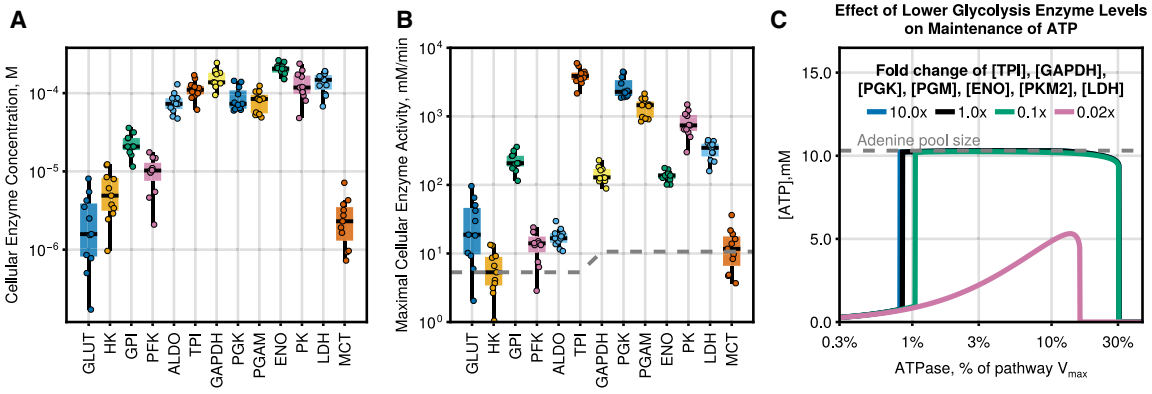

FIGURE 6 Excess activity of glycolytic enzymes relative to HK and PFK is required to maintain high ATP levels. (*A*) Cytosolic enzyme concentrations in the model estimated from proteomics data. (*B*) Maximal cytosolic enzyme activities in the model. Activities of all isoforms for each enzyme were summed together. The dashed line indicates the activity for each enzyme that matches the maximal activity of the slowest enzyme HK1 corrected for the stoichiometry of reactions. (*C*) Steady-state ATP concentrations at a range of ATPase rates of the glycolysis model with scaled concentrations of lower glycolysis enzymes TPI, GAPDH, PGK, PGAM, ENO, PK, and LDH. Julia code to reproduce this figure is available at https://github.com/DenisTitovLab/CellMetabolism.jl.

Please cite this article in press as: Choe et al., Glycolysis model shows that allostery maintains high ATP and limits accumulation of intermediates, Biophysical Journal (2025), https://doi.org/10.1016/j.bpj.2025.03.037

ATP-consuming enzyme 1, ATP-producing enzyme 2, and ATPase, which represents upper glycolysis from HK to ALDO, lower glycolysis from GAPDH to LDH, and cellular ATPase activity, respectively (Fig. 7 *A*):

Enzyme 1: $G + ATP \rightleftarrows XP + ADP$

Enzyme 2: $XP + Phosphate + 2ADP \rightleftarrows L + 2ATP$

ATPase: $ATP + H_2O \rightleftarrows Phosphate + ADP$

Note that metabolite XP, which represents all intracellular glycolysis intermediates, is phosphorylated to conserve phosphate in each step.

To simplify the analysis, we described the kinetics of enzyme 2 and ATPase using modified reversible Michaelis-Menten equations, assuming that enzyme 2 and ATPase are saturated with substrates (54). For enzyme 1, we used the MWC model to add allosteric activation by ADP and phosphate and allosteric inhibition by ATP. We assumed that ADP and phosphate only bind to active conformation, ATP only binds to inactive conformation, inactive MWC conformation of enzyme 1 is catalytically inactive, and regulatory and catalytic sites are saturated with regulators and substrates. The resulting two-enzyme model is described using the following rate equations (see materials and methods for additional detail on the derivation of the two-enzyme model rate equations):

$$V^{Enz\ 1} = \frac{V_{max}^{Enz\ 1}}{\left(1 + \left(\frac{L[ATP]}{[ADP][Phosphate]}\right)^{n}\right)} \left(1 - \frac{1}{K_{eq}^{Enz\ 1}} \frac{[XP][ADP]}{[G][ATP]}\right) \tag{16}$$

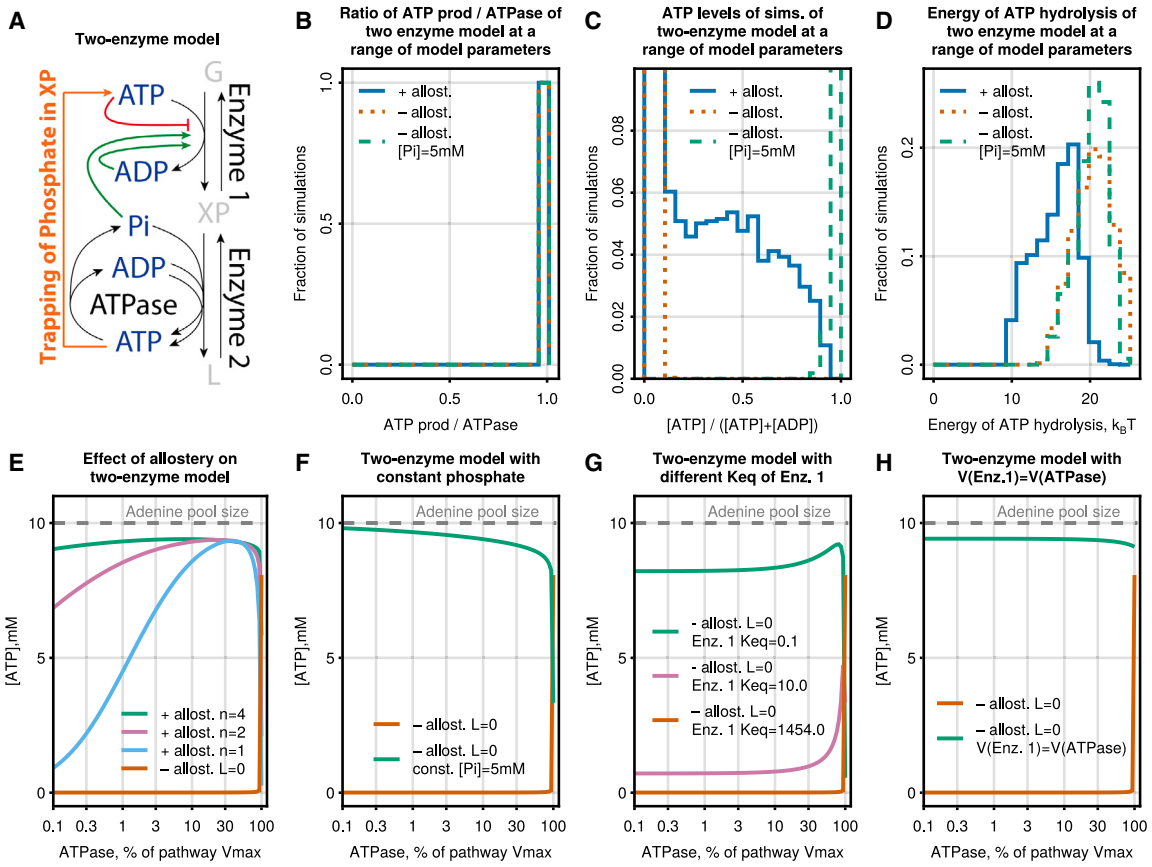

FIGURE 7 Coarse-grained model of glycolysis recapitulates key tasks of ATP homeostasis. (*A*) Schematic of a simplified glycolysis-like pathway containing two enzymes with feedback on Enzyme 1. (B–D) Simulation of the two-enzyme model at random values of the six parameters controlling this pathway showing the ability to (*B*) match ATP supply and demand, (*C*) maintain ATP levels in relation to ATP+ADP, and (*D*) generate energy from ATP hydrolysis. Random values for parameters were taken from log-uniform distributions in the interval of $[10^{-5}, 10^{-1}]$ for L, $[10^{-3}, 10^{-1}]$ for V_{max}, and $[10^{1}, 10^{4}]$ for K_{eq}. Parameters controlling ATPase were not varied, and n was randomly chosen from a set [1, 2, 3, 4]. (*E–H*) Simulation of the two-enzyme with best-performing parameters from (*C*) showing maintenance of steady-state ATP levels at a 100× range of ATPase rates with (*E*) presence and absence of allostery, (*F*) constant inorganic phosphate levels, (*G*) different K_{eq} for enzyme 1 and (*H*) rate of enzyme 1 equal to rate of ATPase. Julia code to reproduce this figure is available at https://github.com/DenisTitovLab/CellMetabolism.jl.

Please cite this article in press as: Choe et al., Glycolysis model shows that allostery maintains high ATP and limits accumulation of intermediates, Biophysical Journal (2025), https://doi.org/10.1016/j.bpj.2025.03.037

$$V^{Enz\ 2} = V_{max}^{Enz\ 2}\left(1 - \frac{1}{K_{eq}^{Enz\ 2}}\frac{[L][ATP]^2}{[XP][ADP]^2[Phosphate]}\right) \quad (17)$$

$$V^{ATPase} = V_{max}^{ATPase}\left(1 - \frac{1}{K_{eq}^{ATPase}}\frac{[ADP][Phosphate]}{[ATP]}\right) \quad (18)$$

Two-enzyme model reduces the number of parameters from >150 for the full model to only 8 for the two-enzyme model, including only two parameters—*L* and *n*—responsible for allosteric regulation. *L* represents the ratio of active to inactive conformation of enzyme 1 in absence of regulators and *n*–oligomeric state of enzyme 1.

We searched for values of the parameters of the two-enzyme model that would support the tasks of ATP homeostasis. We performed 10,000 simulations using random values of two-enzyme model parameters with or without allostery to see which combinations of parameters can support the tasks at a range of ATPase values (Fig. 7, *B–D*). All the parameter combinations could match ATP supply and demand and maintain the energy of ATP hydrolysis >9 k_BT in the presence or absence of allostery, confirming that mass action alone is fully capable of supporting these two tasks (Fig. 7, *B* and *D*). By contrast, only a small fraction of simulations in the presence of allostery and none of the simulations in the absence of allostery could maintain ATP > ADP (Fig. 7 *C*). As for the full model (Fig. 5 *C*), keeping the phosphate level constant abrogated the requirement for allostery for maintaining high ATP levels, confirming that maintenance of ATP > ADP is a nontrivial task that requires allostery to inhibit the reaction of Harden and Young (Fig. 7, *C* and *F*).

We next performed simulations of the two-enzyme model with the parameters that supported the highest level of ATP at a range of ATPase values. We found that removing allostery by setting $L = 0$ completely abrogated while decreasing *n* from 4 to 1 attenuated ATP level maintenance (Fig. 7 *E*). The effect of *n* suggests an important physiological role for the oligomeric structure of allosteric enzymes such as PFKP. As for the full model (Fig. 5 *D*), decreasing the equilibrium constant of enzyme 1 abrogated the requirement for allostery as the trapping of phosphate in XP is less thermodynamically favorable under these conditions (Fig. 7 *G*). It is noteworthy that the two-enzyme model without allostery could maintain ATP > ADP under one exact condition when the $V_{max}^{Enz\ 1} = V_{max}^{ATPase}$ (*red line* in Fig. 7 *E* at 100% ATPase rate)—a condition when the trapping of phosphate is impossible as all of the enzyme 1 capacity is used to satisfy ATP demand with no spare capacity to catalyze the trapping reaction. Finally, as for the full model (Fig. 5 *E*), making $V_{max}^{Enz\ 1} = V_{max}^{ATPase}$ abrogated the requirement for allostery (Fig. 7 *H*). The latter again highlights that allostery prevents the trapping of phosphate by adjusting $V_{max}^{Enz\ 1}$ such that $V_{max}^{Enz\ 1} = V_{max}^{ATPase}$ at a large range of V_{max}^{ATPase}.

It is noteworthy that a higher Hill coefficient allows allosteric regulators to inhibit enzymes to a much greater extent in the presence of high levels of inhibitor due to the $1/[Inhibitor/K_{Inhibitor}]^4$ term, while simultaneously minimizing the effect of low concentrations of inhibitor. The identical effect would be observed for activators but in the opposite direction. Thus, higher Hill coefficient extends the range where allosteric regulation can match HK and PFK rate to one-half of ATPase, perhaps explaining why many allosterically regulated enzymes evolved to have high Hill coefficients.

Overall, our analysis of the two-enzyme model confirms the results of the full model that allosteric regulation is required to maintain high ATP levels, while mass action alone is sufficient to match ATP supply and demand and to ensure that ATP hydrolysis generates energy.

DISCUSSION

Metabolic homeostasis is an emergent property of the activities of many individual enzymes. Regulation of metabolic pathways has historically been studied by rigorously characterizing enzymes in isolation. While this has greatly advanced our understanding of the key regulatory enzymes, many emergent functions of metabolic networks are difficult to understand by focusing on one enzyme at a time. Approaches that combine theory and experiments can explore how the activities of individual enzymes give rise to metabolic homeostasis. Here, we developed a biophysical model of glycolysis that uses enzyme rate equations to describe the activity of the whole glycolysis pathway and applied it to identify the regulatory mechanisms that allow glycolysis to perform the tasks of ATP homeostasis (Fig. 1 *A*). The resulting model can quantitatively predict the output of glycolysis in response to perturbations of metabolite levels and kinetic properties of enzymes, such as changes in media conditions, enzyme expression, drug treatment, and expression of enzyme mutants. Nevertheless, the current model only describes glycolysis of rapidly proliferating cells in the absence of branching pathways, so its predictions outside these conditions should be interpreted cautiously.

One of the remarkable properties of ATP homeostasis is that it can maintain stable ATP levels even when a cell's demand increases by up to 100-fold, while concentrations of intermediates change only 2- to -3-fold (4–6). Given that a classical Michaelis-Menten enzyme rate equation would require a >100-fold change in substrate concentration in the absence of product to achieve 100-fold change in rate, it has been debated whether ATP homeostasis is achieved through feedback sensing of changes in ATP, ADP, and phosphate levels that result from ATP consumption or whether additional mechanisms such as feedforward

Please cite this article in press as: Choe et al., Glycolysis model shows that allostery maintains high ATP and limits accumulation of intermediates, Biophysical Journal (2025), https://doi.org/10.1016/j.bpj.2025.03.037

activation of ATP-producing enzymes by Ca^{2+} are required (72,73). The ability of our model to maintain stable ATP levels at >30-fold changes in the ATP demand, suggests that known in vitro enzyme kinetic properties of glycolytic enzymes are already sufficient to maintain ATP homeostasis in response to changes in ATP, ADP, and phosphate concentrations due to ATP hydrolysis.

Glycolysis is regulated by a combination of mass action and allostery, but it is not fully understood which tasks of ATP homeostasis (Fig. 1 *A*) require mass action versus allostery. We showed that mass action alone is sufficient to match ATP supply and demand, as well as to maintain ATP, ADP, and inorganic phosphate concentrations so that ATP hydrolysis generates energy (Figs. 3 and 7). The capacity of coarse-grained models of glycolysis with only two to three reactions to respond to changes in ATP demand and maintain a high ATP/ADP ratio without allosteric feedback has previously been reported (15), and we confirm these findings using a full-scale model of glycolysis. The key role of mass action can be seen in the stoichiometry of the net reaction of glycolysis:

$$Glucose + 2ADP + 2Phosphate \rightleftarrows 2Lactic\ Acid + 2ATP \quad (19)$$

An increase in ATP consumption rate would push this reaction forward by mass action due to a decrease in the product (ATP) and an increase in substrate levels (ADP and phosphate) resulting from ATP hydrolysis. Likewise, the ATP hydrolysis reaction will be maintained far from equilibrium as long as the net reaction of glycolysis is thermodynamically favorable and can proceed faster than ATP hydrolysis. Thus, the ability of glycolysis to match ATP supply and demand and maintain ATP hydrolysis far from equilibrium is built into the glycolytic pathway, and it is largely independent of the kinetic properties of individual enzymes.

Mass action alone is not sufficient to perform all tasks of ATP homeostasis. We showed that the allosteric regulation of HK1 and PFKP by G6P, ATP, ADP, and Pi is required to maintain most of the adenine nucleotide pool in the form of ATP and prevent the uncontrolled accumulation of phosphorylated intermediates in upper glycolysis (Figs. 3, 5, and 7). The latter is an especially difficult task due to the structure of the glycolysis pathway that gives rise to the thermodynamically favorable reaction of Harden and Young (Fig. 5 *A* and Reaction in Eq. 15), which converts glucose and phosphate into F16BP without a net change in ATP levels. This reaction presents the cell with an impossible choice. If the cell stops the uptake of extracellular phosphate, then cells cannot maintain high ATP levels as phosphate produced by ATP hydrolysis due to normal cellular functions will be trapped in phosphorylated intermediates of glycolysis. Conversely, if the cell continues to uptake extracellular phosphate, then F16BP would accumulate to levels well above the estimated total concertation of intracellular small molecules of 200 mM. Neither option is likely to be compatible with a living cell. We have demonstrated that the allosteric regulation works by reducing HK1 and PFKP reaction rates to the minimal levels necessary to meet ATP demand. This regulation ensures that there is no excess catalytic activity of HK1 and PFKP available to catalyze the reaction of Harden and Young (Fig. 5 *A*).

Multiple experimental observations support the existence of the reaction of Harden and Young and the requirement of allosteric feedback to inhibit it. The reaction was directly observed in 1906 in cell-free alcoholic fermentation of yeast extracts (18), predating the discovery of ATP and the physiologically relevant ATP-producing glycolysis reaction. Meyerhof later demonstrated that the reaction of Harden and Young only occurs in the absence of ATPases (19,71). At the same time, in the presence of ATPases, the same yeast extract starts to catalyze the physiologically relevant ATP-producing reaction of glycolysis. This experimental observation mirrors our model predictions that, even in the presence of allostery, the phosphate trap reaction is predicted to occur if ATPase rate is very low (Fig. 3 *E*, vertical drop-off of ATP levels at ATPase rates <1% of glycolysis V_{max}). The mechanistic explanation for the latter phenomenon is that, at very low ATPase rates, unrealistically high levels of allosteric inhibitors ATP and G6P will be required to set HK and PFK rates to one-half of the ATPase rate, so the allostery will stop working at low enough ATPase rates. These results also suggest the physiological role of PFK being a tetramer and having a high Hill coefficient as it would allow allosteric regulators to set the rate of PFK to one-half of ATPase at a wider range of ATP demands, as discussed in the results and shown in Fig. 7 *E*. The reaction of Harden and Young has also been observed in living cells under some conditions, although it was not referred to by its original name. It has long been known that *S. cerevisiae* mutant Δtps1 lacking trehalose-6-phosphate (T6P) synthase is defective for growth on glucose (20). In the presence of glucose, Δtps1 stops growing and accumulates large amounts of phosphorylated glycolytic intermediates upstream of GAPDH while having depleted levels of ATP, inorganic phosphate, and phosphorylated glycolytic intermediates downstream of GAPDH (20), mimicking our model predictions in the absence of allostery (Fig. 5, *B* and *C*). It turns out that *S. cerevisiae* HK is feedback inhibited by T6P (74) instead of G6P and, thus, the Δtps1 mutant is likely defective in HK feedback inhibition. Our results show that the lack of HK feedback inhibition is sufficient to break the maintenance of ATP levels and lead to trapping of inorganic phosphate, which would explain the unusual phenotype of Δtps1 mutant. In *T. brucei*, it has been observed that the first seven glycolytic enzymes are compartmentalized in peroxisome-like organelles called glycosomes (75), while HK and PFK enzymes are not allosterically regulated (76). Glycosome membranes are not permeable to small molecules, so such compartmentalization would be predicted to break up the reaction of Harden and Young and remove the need for allosteric regulation. In the *T. brucei* mutants, where glycolytic enzymes are not targeted to glycosomes, glucose becomes toxic (77) and leads to the

Please cite this article in press as: Choe et al., Glycolysis model shows that allostery maintains high ATP and limits accumulation of intermediates, Biophysical Journal (2025), https://doi.org/10.1016/j.bpj.2025.03.037

accumulation of glycolytic intermediates (21,78). Finally, overexpression of HK2 in proliferating mouse cell line and glucokinase in pancreatic β cells leads to a decrease in ATP levels and an increase in phosphorylated glycolytic intermediates (22,79), once again mimicking our model prediction (Figs. 5 *C* and 6 *C*).

Our work clarifies the function of some of the most well-known allosteric regulators of a metabolic pathway. To our knowledge, this is the first study to implicate the allosteric regulation of HK and PFK by ATP, ADP, Pi, and G6P in inhibiting the reaction of Harden and Young, despite both being known for over 50 years. Previous research utilizing a coarse-grained model of glycolysis with three enzymes (17) suggested that feedback inhibition of HK by G6P (or T6P in *S. cerevisiae*) may protect cells from an overly active ATP-consuming upper part of glycolysis, which leads to the accumulation of phosphorylated intermediates at the expanse of ATP, as is observed in the Δtps1 mutant. The authors noted that lowering HK expression might achieve a similar outcome, implying that allosteric regulation may only be required under specific conditions, such as high glucose concentrations. Building upon this work, our analysis using a model of all glycolytic enzymes shows that the reaction of Harden and Young drives the accumulation of phosphorylated intermediates at the expense of ATP, rather than solely the overactivity of HK and PFK. Moreover, we demonstrate that the reaction of Harden and Young is unavoidable in the absence of regulation and cannot be mitigated by lowering HK expression levels (Fig. 3 *E*). Additionally, we show that allosteric regulation of HK and PFK by ATP, ADP, and Pi—not just G6P—redundantly inhibits the reaction of Harden and Young (Fig. 4).

Glycolytic enzymes are expressed at unusual levels, with GLUT, HK1, PFKP, and MCT having 10–100× less activity than most of the other enzymes (Fig. 6, *A* and *B*). Such an expression pattern is puzzling given that glycolysis cannot proceed faster than its slowest enzymes, so this 10–100× higher expression seems wasteful. Our results provide a mechanistic explanation for this unusual expression pattern by showing that it is required to maintain high and stable ATP levels and to prevent phosphate trapping (Fig. 6 *C*).

Beyond the applications described in this report, our model of glycolysis can be used for a variety of applications. The model can be used to predict the effect of enzyme mutants or simulate the effects of glycolysis-targeting drugs by changing the corresponding kinetic parameters. Global sensitivity analysis (Fig. S4) can be used to identify key kinetic parameters that control the output of glycolysis, such as the tasks of ATP homeostasis or a concentration of a specific metabolite. The rate equations for glycolytic enzymes can be used to simulate reaction-diffusion systems and investigate the effect of the 3D distribution of glycolytic enzymes. The existence of novel regulators not included in the current model can be inferred by investigating the quantitative differences between model prediction and data.

Our framework to combine theory and experiments can be readily applied to other metabolic pathways. Enzyme rate equations can be derived from the vast literature of in vitro kinetics data, threading together the individual enzyme behaviors to generate the system's behavior. Our approaches for simulations, global sensitivity analysis, and error propagation of systems of ODEs can be directly applied to other pathways without modification. As with glycolysis, we anticipate that such work will lead to a better understanding of the functions of mass action and allostery in the regulation of metabolic homeostasis.

DATA AND CODE AVAILABILITY

- All data reported in this paper are provided as supporting material, Data S1 and S2.
- All original code required to reproduce all the figures is publicly available at https://github.com/DenisTitovLab/CellMetabolism.jl.

ACKNOWLEDGMENTS

We thank the students and instructors of the 2017 Marine Biological Laboratory course on Physical Biology of the Cell for their comments on the early version of this project, participants of the 2019 Kavli Institute for Theoretical Physics workshop on Cellular Energetics for fruitful discussions, Bradley Webb for discussions about PFK regulation, James Mbata for contributions in identifying code errors, and members of the Titov and Phillips labs for many helpful suggestions. This research used the Savio computational cluster resource provided by the Berkeley Research Computing program at the University of California, Berkeley (supported by the UC Berkeley Chancellor, Vice Chancellor for Research, and Chief Information Officer). Research reported in this publication was supported by the National Institute of General Medical Sciences of the National Institutes of Health under award nos. DP2 GM132933 and R35 GM152114 to D.V.T., and R35 GM118043 to R.P. T.E. is supported by Damon Runyon Cancer Research Foundation Fellowship DRQ 01-20.

AUTHOR CONTRIBUTIONS

Conceptualization, R.P. and D.V.T.; data curation, M.C., T.E., and D.V.T.; methodology, M.C., T.E., and D.V.T.; investigation, M.C., T.E., and D.V.T.; funding acquisition, R.P. and D.V.T.; supervision, R.P. and D.V.T.; writing – original draft, D.V.T.; writing – review & editing, M.C., T.E., R.P., and D.V.T.

DECLARATION OF INTERESTS

The authors declare no competing interests.

SUPPORTING CITATIONS

References (9–11,32,65,80–140) appear in the supporting material.

SUPPORTING MATERIAL

Supporting material can be found online at https://doi.org/10.1016/j.bpj.2025.03.037.

Please cite this article in press as: Choe et al., Glycolysis model shows that allostery maintains high ATP and limits accumulation of intermediates, Biophysical Journal (2025), https://doi.org/10.1016/j.bpj.2025.03.037

REFERENCES

1. DeBerardinis, R. J., and N. S. Chandel. 2020. We need to talk about the Warburg effect. *Nat. Metab.* 2:127–129.
2. King, M. P., and G. Attardi. 1989. Human cells lacking mtDNA: repopulation with exogenous mitochondria by complementation. *Science.* 246:500–503.
3. Titov, D. V., V. Cracan, …, V. K. Mootha. 2016. Complementation of mitochondrial electron transport chain by manipulation of the NAD+/NADH ratio. *Science.* 352:231–235.
4. Sacktor, B. 1970. Regulation of Intermediary Metabolism, with Special Reference to the Control Mechanisms in Insect Flight Muscle. *In* Advances in Insect Physiology. J. W. L. Beament, J. E. Treherne, and V. B. Wigglesworth, eds Academic Press, pp. 267–347.
5. Dobson, G. P., W. S. Parkhouse, and P. W. Hochachka. 1987. Regulation of anaerobic ATP-generating pathways in trout fast-twitch skeletal muscle. *Am. J. Physiol.* 253:R186–R194.
6. Hochachka, P. W., M. S. Bianconcini, …, G. P. Dobson. 1991. On the role of actomyosin ATPases in regulation of ATP turnover rates during intense exercise. *Proc. Natl. Acad. Sci. USA.* 88:5764–5768.
7. Pardee, A. B., and R. A. Yates. 1956. Control of pyrimidine biosynthesis in Escherichia coli by a feed-back mechanism. *J. Biol. Chem.* 221:757–770.
8. Umbarger, H. E. 1956. Evidence for a negative-feedback mechanism in the biosynthesis of isoleucine. *Science.* 123:848.
9. Monod, J., J. Wyman, and J.-P. Changeux. 1965. On the nature of allosteric transitions: A plausible model. *J. Mol. Biol.* 12:88–118.
10. Koshland, D. E., G. Némethy, and D. Filmer. 1966. Comparison of experimental binding data and theoretical models in proteins containing subunits. *Biochemistry.* 5:365–385.
11. Phillips, R. 2020. The Molecular Switch. Princeton University Press.
12. Hofmeyr, J. H. 1995. Metabolic regulation: a control analytic perspective. *J. Bioenerg. Biomembr.* 27:479–490.
13. Alon, U. 2019. An Introduction to Systems Biology, 2nd edition. Chapman and Hall/CRC, Boca Raton, Fla.
14. El-Samad, H. 2021. Biological feedback control—Respect the loops. *Cell Syst.* 12:477–487.
15. Sel'kov, E. E. 1975. Stabilization of energy charge, generation of oscillations and multiple steady states in energy metabolism as a result of purely stoichiometric regulation. *Eur. J. Biochem.* 59:151–157.
16. Boiteux, A., B. Hess, and E. E. Sel'kov. 1984. Experimental and Theoretical Studies of the Regulatory Hierarchy in Glycolysis. *In* Self-Organization Autowaves and Structures Far from Equilibrium. V. I. Krinsky, ed Springer Berlin Heidelberg, Berlin, Heidelberg, pp. 240–251.
17. Teusink, B., M. C. Walsh, …, H. V. Westerhoff. 1998. The danger of metabolic pathways with turbo design. *Trends Biochem. Sci.* 23:162–169.
18. Harden, A., W. J. Young, and C. J. Martin. 1906. The alcoholic ferment of yeast-juice. *Proc. R. Soc. Lond. - Ser. B Contain. Pap. a Biol. Character.* 77:405–420.
19. Meyerhof, O. 1945. THE ORIGIN OF THE REACTION OF HARDEN AND YOUNG IN CELL-FREE ALCOHOLIC FERMENTATION. *J. Biol. Chem.* 157:105–119.
20. Van Aelst, L., S. Hohmann, …, P. Coccetti. 1993. Molecular cloning of a gene involved in glucose sensing in the yeast Saccharomyces cerevisiae. *Mol. Microbiol.* 8:927–943.
21. Haanstra, J. R., A. van Tuijl, …, B. M. Bakker. 2008. Compartmentation prevents a lethal turbo-explosion of glycolysis in trypanosomes. *Proc. Natl. Acad. Sci. USA.* 105:17718–17723.
22. Wang, H., and P. B. Iynedjian. 1997. Acute glucose intolerance in insulinoma cells with unbalanced overexpression of glucokinase. *J. Biol. Chem.* 272:25731–25736.
23. Sel'kov, E. E. 1968. Self-oscillations in glycolysis. 1. A simple kinetic model. *Eur. J. Biochem.* 4:79–86.
24. Goldbeter, A., and R. Lefever. 1972. Dissipative Structures for an Allosteric Model: Application to Glycolytic Oscillations. *Biophys. J.* 12:1302–1315.
25. Chandra, F. A., G. Buzi, and J. C. Doyle. 2011. Glycolytic oscillations and limits on robust efficiency. *Science.* 333:187–192.
26. Chance, B. 1952. Spectra and Reaction Kinetics of Respiratory Pigments of Homogenized and Intact Cells. *Nature.* 169:215–221.
27. Ghosh, A., and B. Chance. 1964. Oscillations of glycolytic intermediates in yeast cells. *Biochem. Biophys. Res. Commun.* 16:174–181.
28. Joshi, A., and B. O. Palsson. 1990. Metabolic dynamics in the human red cell. Part IV–Data prediction and some model computations. *J. Theor. Biol.* 142:69–85.
29. Mulquiney, P. J., and P. W. Kuchel. 1999. Model of 2,3-bisphosphoglycerate metabolism in the human erythrocyte based on detailed enzyme kinetic equations: equations and parameter refinement. *Biochem. J.* 342:581–596.
30. van Heerden, J. H., M. T. Wortel, …, B. Teusink. 2014. Lost in transition: start-up of glycolysis yields subpopulations of nongrowing cells. *Science.* 343:1245114.
31. Shestov, A. A., X. Liu, …, J. W. Locasale. 2014. Quantitative determinants of aerobic glycolysis identify flux through the enzyme GAPDH as a limiting step. *Elife.* 3:e03342.
32. Marzen, S., H. G. Garcia, and R. Phillips. 2013. Statistical Mechanics of Monod–Wyman–Changeux (MWC) Models. *J. Mol. Biol.* 425:1433–1460.
33. Einav, T., L. Mazutis, and R. Phillips. 2016. Statistical Mechanics of Allosteric Enzymes. *J. Phys. Chem. B.* 120:6021–6037.
34. Geiger, T., A. Wehner, …, M. Mann. 2012. Comparative proteomic analysis of eleven common cell lines reveals ubiquitous but varying expression of most proteins. *Mol. Cell. Proteomics.* 11:014050.
35. Wiśniewski, J. R., M. Y. Hein, …, M. Mann. 2014. A "proteomic ruler" for protein copy number and concentration estimation without spike-in standards. *Mol. Cell. Proteomics.* 13:3497–3506.
36. Milo, R. 2013. What is the total number of protein molecules per cell volume? A call to rethink some published values. *Bioessays.* 35:1050–1055.
37. Heinrich, L., D. Bennett; …, COSEM Project Team. 2021. Whole-cell organelle segmentation in volume electron microscopy. *Nature.* 599:141–146.
38. Luby-Phelps, K. 2000. Cytoarchitecture and physical properties of cytoplasm: volume, viscosity, diffusion, intracellular surface area. *Int. Rev. Cytol.* 192:189–221.
39. Ellis, R. J. 2001. Macromolecular crowding: obvious but underappreciated. *Trends Biochem. Sci.* 26:597–604.
40. Park, J. O., S. A. Rubin, …, J. D. Rabinowitz. 2016. Metabolite concentrations, fluxes and free energies imply efficient enzyme usage. *Nat. Chem. Biol.* 12:482–489.
41. Chen, W. W., E. Freinkman, …, D. M. Sabatini. 2016. Absolute Quantification of Matrix Metabolites Reveals the Dynamics of Mitochondrial Metabolism. *Cell.* 166:1324–1337.e11.
42. Edwards, J. S., and B. O. Palsson. 2000. Multiple steady states in kinetic models of red cell metabolism. *J. Theor. Biol.* 207:125–127.
43. Xie, J., C. Dai, and X. Hu. 2016. Evidence That Does Not Support Pyruvate Kinase M2 (PKM2)-catalyzed Reaction as a Rate-limiting Step in Cancer Cell Glycolysis. *J. Biol. Chem.* 291:8987–8999.
44. Yurkovich, J. T., D. C. Zielinski, …, B. O. Palsson. 2017. Quantitative time-course metabolomics in human red blood cells reveal the temperature dependence of human metabolic networks. *J. Biol. Chem.* 292:19556–19564.
45. Røst, L. M., L. Brekke Thorfinnsdottir, …, P. Bruheim. 2020. Absolute Quantification of the Central Carbon Metabolome in Eight Commonly Applied Prokaryotic and Eukaryotic Model Systems. *Metabolites.* 10:74.

46. Rackauckas, C., and Q. Nie. 2017. DifferentialEquations.jl – A Performant and Feature-Rich Ecosystem for Solving Differential Equations in Julia. *J. Open Res. Software.* 5:15.
47. Danisch, S., and J. Krumbiegel. 2021. Makie.jl: Flexible high-performance data visualization for Julia. *J. Open Source Softw.* 6:3349.
48. Kacser, H., and J. A. Burns. 1973. The control of flux. *Symp. Soc. Exp. Biol.* 27:65–104.
49. Heinrich, R., and T. A. Rapoport. 1974. A linear steady-state treatment of enzymatic chains. General properties, control and effector strength. *Eur. J. Biochem.* 42:89–95.
50. Saltelli, A. 2008. Global Sensitivity Analysis: The Primer, 1st edition. Wiley-Interscience, Chichester, England; Hoboken, NJ.
51. Saltelli, A., S. Tarantola, …, M. Ratto. 2004. Sensitivity Analysis in Practice: A Guide to Assessing Scientific Models. Halsted Press.
52. Dixit, V. K., and C. Rackauckas. 2022. GlobalSensitivity.jl: Performant and Parallel Global Sensitivity Analysis with Julia. *J. Open Source Softw.* 7:4561.
53. Reich, J., E. Selkov, …, E. E. Selkov. 1981. Energy Metabolism of the Cell. Academic Press, London.
54. Noor, E., A. Flamholz, …, R. Milo. 2013. A note on the kinetics of enzyme action: a decomposition that highlights thermodynamic effects. *FEBS Lett.* 587:2772–2777.
55. Milo, R., and R. Phillips. 2015. Cell Biology by the Numbers, 1st edition. Garland Science, New York, NY.
56. Balaban, R. S., H. L. Kantor, …, R. W. Briggs. 1986. Relation between work and phosphate metabolite in the in vivo paced mammalian heart. *Science.* 232:1121–1123.
57. Allen, P. S., G. O. Matheson, …, P. W. Hochachka. 1997. Simultaneous 31P MRS of the soleus and gastrocnemius in Sherpas during graded calf muscle exercise. *Am. J. Physiol.* 273:R999–R1007.
58. Knight, Z. A., and K. M. Shokat. 2005. Features of Selective Kinase Inhibitors. *Chem. Biol.* 12:621–637.
59. Hackney, D. D., and P. K. Clark. 1985. Steady state kinetics at high enzyme concentration. The myosin MgATPase. *J. Biol. Chem.* 260:5505–5510.
60. Soltoff, S. P., and L. J. Mandel. 1984. Active ion transport in the renal proximal tubule. III. The ATP dependence of the Na pump. *J. Gen. Physiol.* 84:643–662.
61. Atkinson, D. E. 1968. The energy charge of the adenylate pool as a regulatory parameter. Interaction with feedback modifiers. *Biochemistry.* 7:4030–4034.
62. ATKINSON, D. E. 1969. *In* Limitation of Metabolite Concentrations and the Conservation of Solvent Capacity in the Living Cell, B. L. Horecker and E. R. Stadtman, eds Academic Press, pp. 29–43.
63. Savageau, M. A. 1976. Biochemical Systems Analysis: A Study of Function and Design in Molecular Biology. Addison-Wesley Publishing Company, Advanced Book Program.
64. Barkai, N., and S. Leibler. 1997. Robustness in simple biochemical networks. *Nature.* 387:913–917.
65. Beber, M. E., M. G. Gollub, …, E. Noor. 2022. eQuilibrator 3.0: a database solution for thermodynamic constant estimation. *Nucleic Acids Res.* 50:D603–D609.
66. Bezanson, J., A. Edelman, …, V. B. Shah. 2015. Julia: A Fresh Approach to Numerical Computing. Preprint at arXiv. https://doi.org/10.48550/arXiv:1411.1607.
67. Transtrum, M. K., B. B. Machta, …, J. P. Sethna. 2015. Perspective: Sloppiness and emergent theories in physics, biology, and beyond. *J. Chem. Phys.* 143:010901.
68. Kukurugya, M. A., and D. V. Titov. 2024. The Warburg Effect is the result of faster ATP production by glycolysis than respiration. *Proc. Natl. Acad. Sci. USA.* 121:e2409509121.
69. Williamson, D. H., P. Lund, and H. A. Krebs. 1967. The redox state of free nicotinamide-adenine dinucleotide in the cytoplasm and mitochondria of rat liver. *Biochem. J.* 103:514–527.
70. Hung, Y. P., J. G. Albeck, …, G. Yellen. 2011. Imaging Cytosolic NADH-NAD+ Redox State with a Genetically Encoded Fluorescent Biosensor. *Cell Metab.* 14:545–554.
71. Meyerhof, O. 1949. Further studies on the Harden-Young effect in alcoholic fermentation of yeast preparations. *J. Biol. Chem.* 180:575–586.
72. Beard, D. A., and M. J. Kushmerick. 2009. Strong Inference for Systems Biology. *PLoS Comput. Biol.* 5:e1000459.
73. Balaban, R. S. 1990. Regulation of oxidative phosphorylation in the mammalian cell. *Am. J. Physiol.* 258:C377–C389.
74. Blázquez, M. A., R. Lagunas, …, J. M. Gancedo. 1993. Trehalose-6-phosphate, a new regulator of yeast glycolysis that inhibits hexokinases. *FEBS Lett.* 329:51–54.
75. Opperdoes, F. R., and P. Borst. 1977. Localization of nine glycolytic enzymes in a microbody-like organelle in Trypanosoma brucei: the glycosome. *FEBS Lett.* 80:360–364.
76. Nwagwu, M., and F. R. Opperdoes. 1982. Regulation of glycolysis in Trypanosoma brucei: hexokinase and phosphofructokinase activity. *Acta Trop.* 39:61–72.
77. Furuya, T., P. Kessler, …, M. Parsons. 2002. Glucose is toxic to glycosome-deficient trypanosomes. *Proc. Natl. Acad. Sci. USA.* 99:14177–14182.
78. Bakker, B. M., F. I. Mensonides, …, H. V. Westerhoff. 2000. Compartmentation protects trypanosomes from the dangerous design of glycolysis. *Proc. Natl. Acad. Sci. USA.* 97:2087–2092.
79. Tanner, L. B., A. G. Goglia, …, J. D. Rabinowitz. 2018. Four key steps control glycolytic flux in mammalian cells. *Cell Syst.* 7:49–62.e8.
80. Blangy, D., H. Buc, and J. Monod. 1968. Kinetics of the allosteric interactions of phosphofructokinase from Escherichia coli. *J. Mol. Biol.* 31:13–35.
81. Rohatgi, A. 2022. WebPlotDigitizer. https://automeris.io/docs/#citewebplotdigitizer.
82. Lowe, A. G., and A. R. Walmsley. 1986. The kinetics of glucose transport in human red blood cells. *Biochim. Biophys. Acta.* 857:146–154.
83. Wilson, J. E. 2003. Isozymes of mammalian hexokinase: structure, subcellular localization and metabolic function. *J. Exp. Biol.* 206:2049–2057.
84. Copley, M., and H. J. Fromm. 1967. Kinetic studies of the brain hexokinase reaction. A reinvestigation with the solubilized bovine enzyme. *Biochemistry.* 6:3503–3509.
85. Rose, I. A., J. V. Warms, and E. L. O'Connell. 1964. Role of inorganic phosphate in stimulating the glucose utilization of human red blood cells. *Biochem. Biophys. Res. Commun.* 15:33–37.
86. Rijksen, G., and G. E. Staal. 1977. Regulation of human erythrocyte hexokinase. The influence of glycolytic intermediates and inorganic phosphate. *Biochim. Biophys. Acta.* 485:75–86.
87. Chakrabarti, U., and U. W. Kenkare. 1974. Dimerization of brain hexokinase induced by its regulator glucose 6-phosphate. *J. Biol. Chem.* 249:5984–5988.
88. Wilson, J. E. 1973. Ligand-induced conformations of rat brain hexokinase: effects of glucose-6-phosphate and inorganic phosphate. *Arch. Biochem. Biophys.* 159:543–549.
89. Redkar, V. D., and U. W. Kenkare. 1972. Bovine Brain Mitochondrial Hexokinase. *J. Biol. Chem.* 247:7576–7584.
90. Ardehali, H., R. L. Printz, …, D. K. Granner. 1999. Functional interaction between the N- and C-terminal halves of human hexokinase II. *J. Biol. Chem.* 274:15986–15989.
91. Fang, T. Y., O. Alechina, …, R. B. Honzatko. 1998. Identification of a phosphate regulatory site and a low affinity binding site for glucose 6-phosphate in the N-terminal half of human brain hexokinase. *J. Biol. Chem.* 273:19548–19553.
92. Liu, X., C. S. Kim, …, H. J. Fromm. 1999. Dual Mechanisms for Glucose 6-Phosphate Inhibition of Human Brain Hexokinase. *J. Biol. Chem.* 274:31155–31159.

93. Mehta, A., G. K. Jarori, and U. W. Kenkare. 1988. Brain hexokinase has no preexisting allosteric site for glucose 6-phosphate. *J. Biol. Chem.* 263:15492–15497.

94. Chou, A. C., and J. E. Wilson. 1974. Rat brain hexokinase: glucose and glucose-6-phosphate binding sites and C-terminal amino acid of the purified enzyme. *Arch. Biochem. Biophys.* 165:628–633.

95. Aleshin, A. E., C. Kirby, …, R. B. Honzatko. 2000. Crystal structures of mutant monomeric hexokinase I reveal multiple ADP binding sites and conformational changes relevant to allosteric regulation. *J. Mol. Biol.* 296:1001–1015.

96. Rosano, C., E. Sabini, …, M. Bolognesi. 1999. Binding of non-catalytic ATP to human hexokinase I highlights the structural components for enzyme-membrane association control. *Structure.* 7:1427–1437.

97. Ureta, T., P. A. Lazo, and A. Sols. 1985. Allosteric inhibition of brain hexokinase by glucose 6-phosphate in the reverse reaction. *Arch. Biochem. Biophys.* 239:315–319.

98. Solheim, L. P., and H. J. Fromm. 1983. Effect of inorganic phosphate on the reverse reaction of bovine brain hexokinase. *Biochemistry.* 22:2234–2239.

99. Ellison, W. R., J. D. Lueck, and H. J. Fromm. 1975. Studies on the mechanism of orthophosphate regulation of bovine brain hexokinase. *J. Biol. Chem.* 250:1864–1871.

100. Ellison, W. R., J. D. Lueck, and H. J. Fromm. 1974. Studies on the kinetics and mechanism of orthophosphate activation of bovine brain hexokinase. *Biochem. Biophys. Res. Commun.* 57:1214–1220.

101. Ning, J., D. L. Purich, and H. J. Fromm. 1969. Studies on the kinetic mechanism and allosteric nature of bovine brain hexokinase. *J. Biol. Chem.* 244:3840–3846.

102. Kosow, D. P., F. A. Oski, …, I. A. Rose. 1973. Regulation of mammalian hexokinase: regulatory differences between isoenzyme I and II. *Arch. Biochem. Biophys.* 157:114–124.

103. Bianchi, M., G. Serafini, …, M. Magnani. 1998. Enzymatic properties of overexpressed human hexokinase fragments. *Mol. Cell. Biochem.* 189:185–193.

104. Lin, H.-Y., Y.-H. Kao, …, M. Meng. 2009. Effects of inherited mutations on catalytic activity and structural stability of human glucose-6-phosphate isomerase expressed in Escherichia coli. *Biochim. Biophys. Acta.* 1794:315–323.

105. Boscá, L., J. J. Aragón, and A. Sols. 1982. Specific activation by fructose 2,6-bisphosphate and inhibition by P-enolpyruvate of ascites tumor phosphofructokinase. *Biochem. Biophys. Res. Commun.* 106:486–491.

106. Tsai, M. Y., and R. G. Kemp. 1974. Rabbit brain phosphofructokinase. Comparison of regulatory properties with those of other phosphofructokinase isozymes. *J. Biol. Chem.* 249:6590–6596.

107. Meienhofer, M. C., D. Cottreau, …, A. Kahn. 1980. Kinetic properties of human F4 phosphofructokinase: a poor regulatory enzyme. *FEBS Lett.* 110:219–222.

108. Fitch, C. D., R. Chevli, and M. Jellinek. 1979. Phosphocreatine does not inhibit rabbit muscle phosphofructokinase or pyruvate kinase. *J. Biol. Chem.* 254:11357–11359.

109. Jenkins, C. M., J. Yang, …, R. W. Gross. 2011. Reversible high affinity inhibition of phosphofructokinase-1 by acyl-CoA: a mechanism integrating glycolytic flux with lipid metabolism. *J. Biol. Chem.* 286:11937–11950.

110. Ui, M. 1966. A role of phosphofructokinase in pH-dependent regulation of glycolysis. *Biochim. Biophys. Acta.* 124:310–322.

111. Reinhart, G. D. 1980. Influence of polyethylene glycols on the kinetics of rat liver phosphofructokinase. *J. Biol. Chem.* 255:10576–10578.

112. Sommercorn, J., T. Steward, and R. A. Freedland. 1984. Activation of phosphofructokinase from rat tissues by 6-phosphogluconate and fructose 2,6-bisphosphate. *Arch. Biochem. Biophys.* 232:579–584.

113. Kemp, R. G., M. Y. Tsai, and G. Colombo. 1976. A kinetic model for phosphofructokinase based on the paradoxical action of effectors. *Biochem. Biophys. Res. Commun.* 68:942–948.

114. Rose, I. A., J. V. Warms, and D. J. Kuo. 1987. Concentration and partitioning of intermediates in the fructose bisphosphate aldolase reaction. Comparison of the muscle and liver enzymes. *J. Biol. Chem.* 262:692–701.

115. Rose, I. A., and E. L. O'Connell. 1969. Studies on the interaction of aldolase with substrate analogues. *J. Biol. Chem.* 244:126–134.

116. Kasprzak, A. A., and M. Kochman. 1980. Interaction of fructose-1,6-bisphosphate aldolase with adenine nucleotides. Binding of 5'-mononucleotides and phosphates to rabbit muscle aldolase. *Eur. J. Biochem.* 104:443–450.

117. Reynolds, S. J., D. W. Yates, and C. I. Pogson. 1971. Dihydroxyacetone phosphate. Its structure and reactivity with -glycerophosphate dehydrogenase, aldolase and triose phosphate isomerase and some possible metabolic implications. *Biochem. J.* 122:285–297.

118. Trentham, D. R., C. H. McMurray, and C. I. Pogson. 1969. The active chemical state of D-glyceraldehyde 3-phosphate in its reactions with D-glyceraldehyde 3-phosphate dehydrogenase, aldolase and triose phosphate isomerase. *Biochem. J.* 114:19–24.

119. Grüning, N.-M., D. Du, …, M. Ralser. 2014. Inhibition of triosephosphate isomerase by phosphoenolpyruvate in the feedback-regulation of glycolysis. *Open Biology.* 4:130232.

120. Smith, C. M., and S. F. Velick. 1972. The glyceraldehyde 3-phosphate dehydrogenases of liver and muscle. Cooperative interactions and conditions for functional reversibility. *J. Biol. Chem.* 247:273–284.

121. Segel, I. 1993. Enzyme Kinetics: Behavior and Analysis of Rapid Equilibrium and Steady-State Enzyme Systems. John Wiley & Sons.

122. Lavoinne, A., J. C. Marchand, …, F. Matray. 1979. [Rat liver phosphoglycerate kinase. I. Purification and kinetic properties in the biosynthesis of 1-3 diphosphoglycerate]. *Biochimie.* 61:1043–1053.

123. Lavoinne, A., J. C. Marchand, …, F. Matray. 1983. Kinetic studies of the reaction mechanism of rat liver phosphoglycerate kinase in the direction of ADP utilization. *Biochimie.* 65:211–220.

124. Lee, C. S., and W. J. O'Sullivan. 1975. Properties and mechanism of human erythrocyte phosphoglycerate kinase. *J. Biol. Chem.* 250:1275–1281.

125. Ali, M., and Y. S. Brownstone. 1976. A study of phosphoglycerate kinase in human erythrocytes. II. Kinetic properties. *Biochim. Biophys. Acta.* 445:89–103.

126. Ferdinand, W. 1966. The interpretation of non-hyperbolic rate curves for two-substrate enzymes. A possible mechanism for phosphofructokinase. *Biochem. J.* 98:278–283.

127. King, E. L. 1956. Unusual Kinetic Consequences of Certain Enzyme Catalysis Mechanisms. *J. Phys. Chem.* 60:1378–1381.

128. Oslund, R. C., X. Su, …, J. D. Rabinowitz. 2017. Bisphosphoglycerate mutase controls serine pathway flux via 3-phosphoglycerate. *Nat. Chem. Biol.* 13:1081–1087.

129. Bartrons, R., and J. Carreras. 1982. Purification and characterization of phosphoglycerate mutase isozymes from pig heart. *Biochim. Biophys. Acta.* 708:167–177.

130. Suzuki, F., Y. Umeda, and K. Kato. 1980. Rat brain enolase isozymes. Purification of three forms of enolase. *J. Biochem.* 87:1587–1594.

131. Yuan, M., I. W. McNae, …, M. D. Walkinshaw. 2018. An allostatic mechanism for M2 pyruvate kinase as an amino-acid sensor. *Biochem. J.* 475:1821–1837.

132. Chaneton, B., P. Hillmann, …, E. Gottlieb. 2012. Serine is a natural ligand and allosteric activator of pyruvate kinase M2. *Nature.* 491:458–462.

133. Pogson, C. I. 1968. Adipose-tissue pyruvate kinase. Properties and interconversion of two active forms. *Biochem. J.* 110:67–77.

134. Nandi, S., M. Razzaghi, …, M. Dey. 2020. Structural basis for allosteric regulation of pyruvate kinase M2 by phosphorylation and acetylation. *J. Biol. Chem.* 295:17425–17440.

135. Liu, V. M., A. J. Howell, …, M. G. Vander Heiden. 2020. Cancer-associated mutations in human pyruvate kinase M2 impair enzyme activity. *FEBS Lett.* 594:646–664.

136. Nagao, Y., T. Toda, …, T. Horio. 1977. Crystallization of spleen-type (M2-type) pyruvate kinase from Rhodamine sarcoma of rats and its properties. *J. Biochem.* 82:1331–1345.

137. Zewe, V., and H. J. Fromm. 1962. Kinetic studies of rabbit muscle lactate dehydrogenase. *J. Biol. Chem.* 237:1668–1675.

138. Wang, C. S. 1977. Inhibition of human erythrocyte lactate dehydrogenase by high concentrations of pyruvate. Evidence for the competitive substrate inhibition. *Eur. J. Biochem.* 78:569–574.

139. Zewe, V., and H. J. Fromm. 1965. KINETIC STUDIES OF RABBIT MUSCLE LACTATE DEHYDROGENASE. II. MECHANISM OF THE REACTION. *Biochemistry.* 4:782–792.

140. Carpenter, L., and A. P. Halestrap. 1994. The kinetics, substrate and inhibitor specificity of the lactate transporter of Ehrlich-Lettre tumour cells studied with the intracellular pH indicator BCECF. *Biochem. J.* 304:751–760.